DESIGN OPTIMIZATION OF AN INDUSTRIAL OVEN HEAT EXCHANGER

A Thesis Submitted to
the Graduate School of Engineering and Science of
İzmir Institute of Technology
in Partial Fulfillment of the Requirements for the Degree of

MASTER OF SCIENCE

in Mechanical Engineering

by
Güven NERGİZ

December 2021
İZMİR

ACKNOWLEDGMENTS

Firstly, I would like to express my sincere gratitude to my advisor Prof. Dr. Erdal ÇETKİN for his inspiring point of view and continuous involvement through my research, even during the pandemic.

I would like to thank Electron Powder Coatings for sharing valuable information and data for use in this study.

And many thanks to BIAS Engineering for their CFD software support and trust in me.

I would like to thank Prof. Dr. Aşkıner GÜNGÖR and Assoc. Prof. Dr. Mehmet Akif EZAN for their guidance and inspiring advices.

Finally, my special thanks to Lütfi NERGİZ, Süheyla NERGİZ, and Serenat DİLBER for their endless support and trust in me.

ABSTRACT

DESIGN OPTIMIZATION OF AN INDUSTRIAL OVEN HEAT EXCHANGER

The coating application of metals (especially in automotive and white goods sectors) is used in various fields to protect the metal against oxidation, corrosion, scratch, or high temperature to increase product lifetime. The most efficient technique in the coating application is powder coating where the powder is Epoxy-polyester. This process has three steps; surface pretreatment (washing), powder coating, and curing the coated metal. Metals may need to be dried and cured in ovens with 90°C and 200°C, respectively, for the required quality coating process. Burners are used as the heat source in the oven's heat exchangers. Due to high temperatures, the expanding heat exchanger is exposed to various thermal stresses. The stresses cause cracking and rupture problems. The regions where thermal stresses occur intensely are the surfaces with high-temperature differences. Various mass flow rates in the heat exchanger cause non-uniformity for how the energy to be transferred, thus non-uniform surface temperature distribution. In this study, a heat exchanger design provided by "ELECTRON – Sistem Teknik Makina" company has been studied. The mass flow rates in the heat transfer pipes (where the heat is mainly transferred) show deviations up to 75% from the ideal rate. With this study, deviations have been reduced to the level of ±10%. The results show that the maximum thermal stress on the heat exchanger was reduced by 24% with this improvement. In general, the uniform mass flow rates obtained in the heat transfer pipes provided a more homogeneous distribution of the surface temperatures, thus decreased thermal stresses.

Keywords: *Industrial Oven, Design Optimization, In-Direct Fired Heat Exchangers*

ÖZET

BİR ENDÜSTRİYEL FIRIN ISI DEĞİŞTİRİCİSİNİN TASARIM OPTİMİZASYONU

Günümüzde metallerin (özellikle otomotiv ve beyaz eşya sektörlerinde) oksitlenme, korozyon, çizik veya yüksek ısıya karşı korunması, ürünün açısından oldukça önemlidir. Tüm bu etkenlere karşı koruma sağlayabilecek en verimli uygulamalardan birisi toz boyama işlemidir. Bu işlem önce metalin yüzeyindeki artık maddelerden arındırılmasıyla başlar, toz kaplanması ile devam eder ve son olarak yüzeyindeki tozun kürlenmesi ile tamamlanmış olur. Bu uygulamada epoksi-polyester malzemeler kullanılmaktadır ve kaliteli bir kaplama işleminin gerçekleştirilmesi için kaplanmış metallerin yaklaşık 90°C'lik fırınlarda kurutulması ve 200°C'lik fırınlarda pişirilmesi gerekebilmektedir. Bu fırınlarda genellikle ısı kaynağı olarak kullanılan brülör, bir fırının değiştiricisine takılır. Yüksek akışkan sıcaklıkları sebebiyle genleşen ısı değiştirici ürünü çeşitli termal gerilmelere maruz kalır. Bu etkiler sonucunda çatlama, kopma gibi problemler yaşanabildiği için termal gerilmelerin azaltılması oldukça önemlidir. Yüksek termal gerilmeler özellikle yüksek sıcaklık farklarının oluştuğu yüzeylerde gözlemlenir. Isı değiştirici içerisindeki farklı akışkan debileri farklı miktarda enerjinin transferine, yani farklı yüzey sıcaklıklarına sebebiyet vermektedir. Bu çalışmada "ELECTRON – Sistem Teknik Makina" firmasının sağlamış olduğu ısı değiştirici (termal gerilmeler sonucunda plastik deformasyon gözlemlendiği) tasarımı içerisinde bulunduğu ortam ile birlikte incelenmiştir. Isının yoğun olarak transfer edildiği borulardaki akışkan debileri başlangıçta olması gereken ideal değerden %75'lere varan sapmalar göstermektedir. Yapılan çalışma ile birlikte bu değer ±%10 mertebesine indirilmiştir. Sonuçlar göstermektedir ki bu iyileştirme ile birlikte ısı değiştirici yüzeyindeki maksimum termal gerilme %24 azaltılmıştır. Genel olarak, ısı değiştiricisi borularında elde edilen homojen akışkan debileri yüzey sıcaklıklarının daha homojen dağılmasını, dolayısıyla termal gerilmelerin azalmasını sağlamıştır.

Anahtar Kelimeler: *Endüstriyel Fırın, Tasarım Optimizasyonu, İndirekt Yanmalı Isı Değiştirici*

TABLE OF CONTENTS

LIST OF FIGURES vi

LIST OF TABLES ix

LIST OF SYMBOLS x

CHAPTER 1 INTRODUCTION 12

1.1. Convection Ovens 13

1.2. Indirect Fired Heat Exchanger 15

CHAPTER 2 NUMERICAL MODEL 19

2.1. Flow Volumes 19

2.2. Outer Walls 21

2.3. Inner Walls (Surfaces) 23

2.4. Conditions 27

2.4.1. Hot Gas Inlet 27

2.5. Setup Properties 32

2.5.1. Current State of the Model 32

2.5.2. Outputs of the Current-State Model 42

CHAPTER 3 RESULTS 50

CHAPTER 4 CONCLUSION 57

REFERENCES 59

LIST OF FIGURES

Figure **Page**

Figure 1.1. Electrostatic powder coating technique 12

Figure 1.2. Typical industrial drying-curing convection oven / ELECTRON Company Internal Report 14

Figure 1.3. The 3D model shape of the convection oven (Figure 1.2) and the cross-section view of the middle plane (with the flow paths of the air inside the oven) / ELECTRON Company Internal Report 14

Figure 1.4. Airflow in the different type curing/drying convection oven / ELECTRON Company Internal Report 15

Figure 1.5. Sections of the Indirect Fired Heat Exchanger with hot gas flow path / ELECTRON Company Internal Report 16

Figure 1.6. Some crack examples on the heat exchanger / ELECTRON Company Internal Report 18

Figure 1.7. Some crack examples on the heat exchanger / ELECTRON Company Internal Report 18

Figure 2.1. Dimensions of the Indirect-Fired Heat Exchanger flow volume (in mm) / ELECTRON Company Internal Report 20

Figure 2.2. Extracting flow volume by considering external and internal flow in the thermoblock / ELECTRON Company Internal Report 20

Figure 2.3. Comparison of flue gas and air for specific heat and density properties by temperature 21

Figure 2.4. Comparison of flue gas and air for viscosity properties by temperature 21

Figure 2.5. Cross-section view of the thermoblock's wall 22

Figure 2.6. Dimensions (radius) of the heat transfer pipe (in mm) 24

Figure 2.7. Dimensions of the outer volume of the heat transfer pipe thermal resistance validation cases 24

Figure 2.8. Thermal resistance validation model – with pipe 26

Figure 2.9. Thermal resistance validation model – without pipe 26

Figure 2.10. Temperature contours where the external flow is in the -y direction; the top is "without pipe", and the bottom is "with pipe" 27

Figure **Page**

Figure 2.11. Measurement of the pressure differences of the chimney gas to obtain volume flow rate of it 28
Figure 2.12. View direction for naming codes and flow directions in the turn sections of the heat transfer pipes 33
Figure 2.13. Cross-section numbering of the pipes due to flow and view direction of "Figure 2.12." 33
Figure 2.14. Flow volumes and flow directions of the current-state case (Cross view) 34
Figure 2.15. Control volumes of the thermoblock component – Front and side view ... 35
Figure 2.16. Control volume of the Indirect Fired Drum & Tube Heat Exchanger – Cross view 35
Figure 2.17. Control volume of the Indirect-Fired Drum & Tube Heat Exchanger – Front and Side views 36
Figure 2.18. Transparent side views of the Indirect-Fired Drum & Tube Heat Exchanger flow volume 36
Figure 2.19. Outer flow volume of the heat exchanger – Cross view 37
Figure 2.20. Outer flow volume of the heat exchanger – Front and side view 37
Figure 2.21. "Hex_inlet" (left) and "hex_outlet" (right) named selections and flow directions of the Heat Exchanger flow volume 38
Figure 2.22. "Wall_hex" (left) and "wall_thermo" (right) named selections of the heat exchanger and thermoblock flow volumes 39
Figure 2.23. "Thermo_inlet" (left) and "thermo_outlet" (right) named selections and flow directions of the thermoblock flow volume 39
Figure 2.24. Hexahedral meshed flow volumes (Front and side view) 41
Figure 2.25. Polyhedral mesh conversion of the flow volumes with boundary layers ... 41
Figure 2.26. Boundary layers of the Polyhedral mesh in the pipe sections 42
Figure 2.27. Convergence graph of the current-state analysis 42
Figure 2.28. Temperature counters of outer surfaces 43
Figure 2.29. Temperature counters of the flow volumes perpendicular to mid-plane 44
Figure 2.30. Flow velocities of the fluid in the heat exchanger 45
Figure 2.31. Surface temperatures of the heat transfer pipes 45
Figure 2.32. Mass flow rates of air in the heat transfer pipes section [Kg/s] 46

Figure **Page**

Figure 2.33. Deviation of the mass flow rates from ideal mass flow rates 46
Figure 2.34. Mass flow rate ratio values in the heat transfer pipes 47
Figure 2.35. Average surface temperatures of the heat transfer pipes (°C) 48
Figure 2.36. Fixed edges (symmetrical) of the heat exchanger for FEA simulation 49
Figure 2.37. FEA thermal stress analysis of the current-state model with maximum stress [Pa] 49
Figure 3.1. Control volume of the optimization study (with mesh) 51
Figure 3.2. Results of the mesh dependency test 51
Figure 3.3. Diameter change ratio of the pipes 52
Figure 3.4. Convergence graph of the improved-state analysis 52
Figure 3.5. Fluid temperatures in the thermoblock and heat exchanger volumes with improved geometry (improved-state) 53
Figure 3.6 Velocity vectors of the outer flow and flow velocities in the heat exchanger (improved-state) 54
Figure 3.7. Mass flow rates of air in the heat transfer pipes section (improved-state) [kg/s] 54
Figure 3.8. Deviation of the flow rates from ideal rates (improved-state) 55
Figure 3.9. Mass flow rate ratio values in the heat transfer pipes (improved-state) 55
Figure 3.10. Average surface temperatures of the heat transfer pipes (improved-state) [°C] 56
Figure 3.11. FEA thermal stress analysis of improved model 56

LIST OF TABLES

Table **Page**

Table 2.1. Properties of thermoblock wall materials for thermal resistance calculation 23
Table 2.2. Thermal properties of P236GH Non-Alloy-Steel 24
Table 2.3. Real-time experimental measurements of the oven by ELECTRON Company 29
Table 2.4. Some thermophysical properties of Natural Gas 30
Table 2.5. Determination of the volumetric flow rate of the Natural Gas in the combustion gases 31
Table 2.6. Determination of the temperature of hot gas inlet to the heat exchanger 32
Table 2.7. Analysis conditions 40
Table 2.8. Outputs of the current-state model 43
Table 2.9. Mechanical properties of P235GH material 48
Table 3.1. Outputs of the improved model 53

LIST OF SYMBOLS

R_{wall}	Thermal resistance of the wall	$m^2.K/W$
h	Heat transfer (convection) coefficient	$W/m^2.K$
k	Heat transfer (conduction) coefficient	W/m.K
r_{Inner}	Inner radius dimension of the pipe	m
r_{Outer}	Outer radius dimension of the pipe	m
Re	Reynolds number	-
L	Length	m
V_{Avg}	Average velocity	m/s
D_H	Hydraulic diameter	m
w	Width	m
T_{Gas}	Gas temperature	°C
P	Pressure	Pa
V, V_{Gas}	Velocity of the fluid	m/s
g	Gravity	m/s^2
h_L	Height from the ground	m
$\dot{Q}$	Heat flow rate	kJ/s
$A_{Chimney}$	Cross-section area of the chimney pipe	m^2
$D_{Chimney}$	Diameter of the chimney pipe	m
$\dot{m}$	Mass flow rate	kg/s
$\dot{V}$	Volumetric flow rate	m^3/s
h	Enthalpy	kJ/kg
N	Number of something	-

Greek Letters

ρ	Density	kg/m^3
μ	Dynamic viscosity	Pa.s
λ	Air ratio	-
Δ	Difference	-

Subscripts

CFD	Computational Fluid Dynamics
HEX	Indirect Fired Heat Exchanger
HV	Heating Value
FEA	Finite Element Analysis

CHAPTER 1

INTRODUCTION

The process of coating metal parts to protect from oxidation, rusting, corrosion, scratching, striking, or attractiveness is critical in the manufacturing sector. Many techniques have been developed to perform the coating process. One of the most widely used techniques is the electrostatic powder coating method, a dry coating process. The basic principle of the technique is based on charging epoxy powder particles and spraying them on a grounded metal part (Figure 1.1) [1]. When the negatively charged particles contact the metal part, they transmit their charge, and a perfect adhesion occurs. One of the reasons for the widespread use of this technique is that a homogeneous coating can be made even on surfaces with the latest geometry. Instead of piling up on each other, the charged epoxy particles move towards the uncoated surfaces of the part in the direction of magnetic effects. Thus, homogeneous coating thickness can be obtained on the part's surface [2].

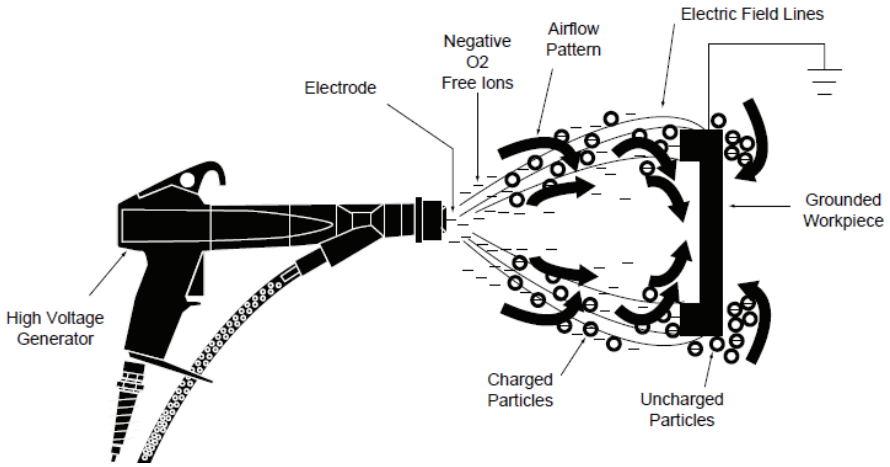

Figure 1.1. Electrostatic powder coating technique [1]

A good quality coating process is a process that includes many applications. Spraying epoxy particles alone is not sufficient for the coating process. For this application to be permanent, the epoxy material must be cured. The epoxy material must be melted for the curing process; usually, the required oven temperature is about 200°C

[3]. However, metal parts are shipped to different locations as raw materials after being produced. For this reason, metals are coated with various chemicals (oil-based, etc.) to prevent them from rusting and oxidation during the shipping process. Of course, this application brings the necessity of an additional application. Because this chemical layer between the surface of the part and the powder coating causes a poor-quality coating process, for this reason, it is necessary to clean the parts (surface treatment) to be coated before the coating process. As a result of a process in which various solvents are used, the chemicals are cleaned from the part's surface [4]. However, moisture and liquid droplets may remain on the part's surface after this process. A drying process is applied to avoid moisture and water droplets remaining on the part's surface.

Both drying and curing processes are carried out in similar ovens with different thermal capacities. These are large industrial ovens, large enough to contain coated parts. Technically, two types of ovens are used in this sector: Infrared and convection. Infrared ovens are preferred because of their easy use and fast application. Infrared rays provide high temperatures on the surfaces they contact with. Infrared rays penetrate only the part without heating the entire air volume in the oven, and it causes the surface of the part to heat up quickly and dry or cure. However, the parts mentioned here are only straight parts without complicated geometry. Because the more complex the parts, the fewer the surfaces that infrared rays can contact. For this reason, the traditional technique with the most common usage is convection ovens.

1.1. Convection Ovens

Convection ovens transfer heat by forced convection, so a good drying/curing process is obtained even if the part is complex. As seen in Figure 1.2., they are placed on the conveyor system that carries the parts. After the parts are placed inside, the doors are closed, and the drying/curing process is performed.

Figure 1.2. Typical industrial drying-curing convection oven / ELECTRON Company Internal Report

The internal temperature of drying ovens starts from approximately 80°C, more so in curing ovens. Heat is transferred to the air inside the oven by passing over a heat exchanger to achieve these temperatures. As seen in Figure 1.3., the region where the parts are located is called the oven interior, and where the hot fluid is obtained is called "thermoblock". Thanks to the circulation fans in the thermoblock, the air inside the oven is first sucked and then passed over the heat exchanger and sent back to the oven interior. Thus, heat is transferred to the cold fluid in the oven, and hot fluid is obtained.

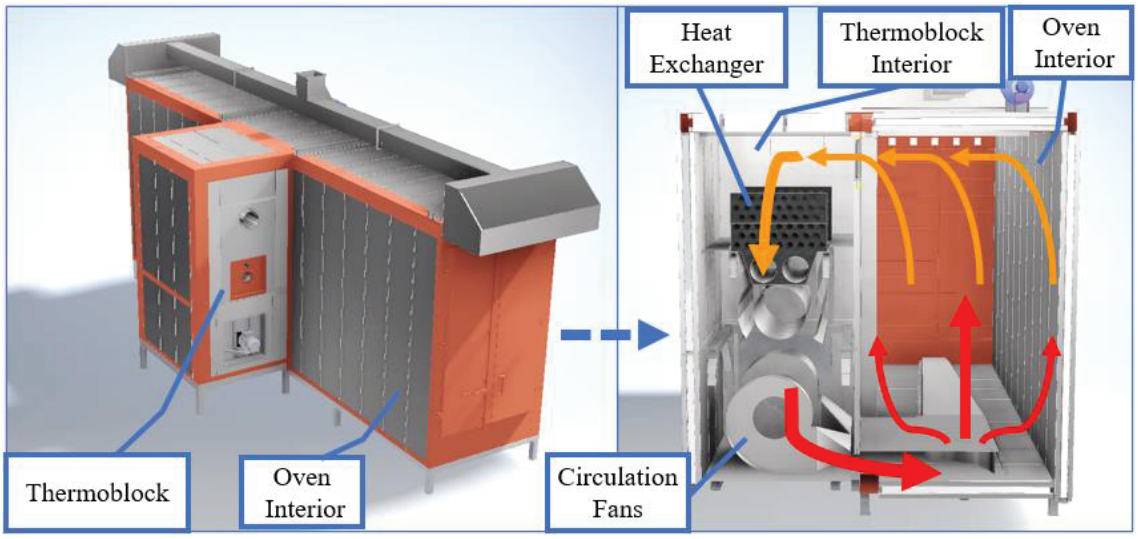

Figure 1.3. The 3D model shape of the convection oven (Figure 1.2) and the cross-section view of the middle plane (with the flow paths of the air inside the oven) / ELECTRON Company Internal Report

The system designs are the same, even if the oven volume or path of the moving parts are changed. For example, Figure 1.4. shows an oven model where the parts first enter the oven and then make a U-turn inside and come out from the same section. The oven model is different, but the working principle is the same.

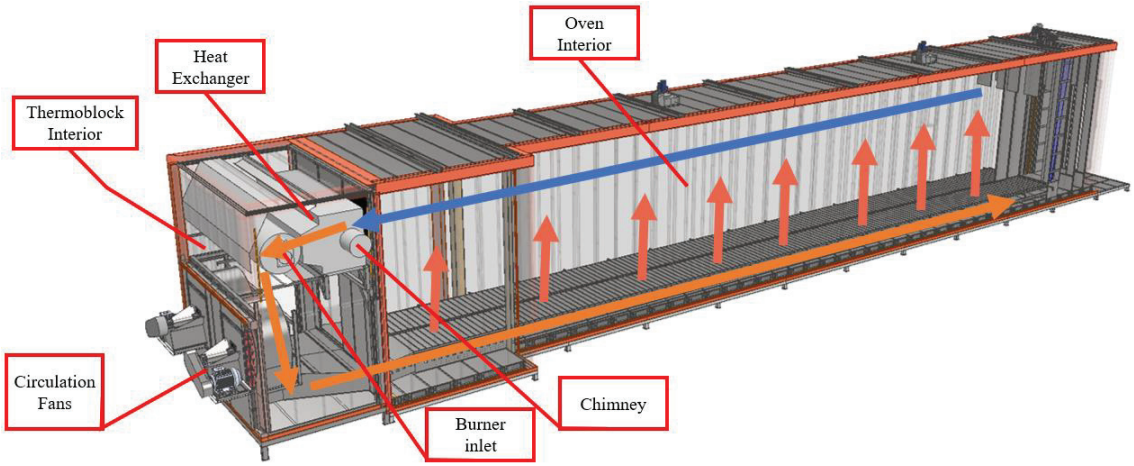

Figure 1.4. Airflow in the different type curing/drying convection oven / ELECTRON Company Internal Report

1.2. Indirect Fired Heat Exchanger

Ovens with internal volumes of various capacities require various amounts of hot air flow to perform the necessary drying/curing process. Heat exchangers with multiple designs are produced to provide various hot air rate needs. The most used heat exchangers in this sector are the Indirect-Fired Drum & Tube Heat Exchangers. These heat exchangers consist of a combustion chamber, smoke pipes, and heat transfer pipes (Figure 1.5.). The burner (liquid or gas fuel), which is the heat source, is mounted at the entrance of the combustion chamber. Here, the flue gases are produced due to the burner flame first following the smoke pipes and then the heat transfer pipes and leaves the heat exchanger from the chimney. During this process, the air inside the oven, which is sucked from the top section by the circulation fans (Figure 1.3.), passes over the heat exchanger and is sent back to the inside of the oven.

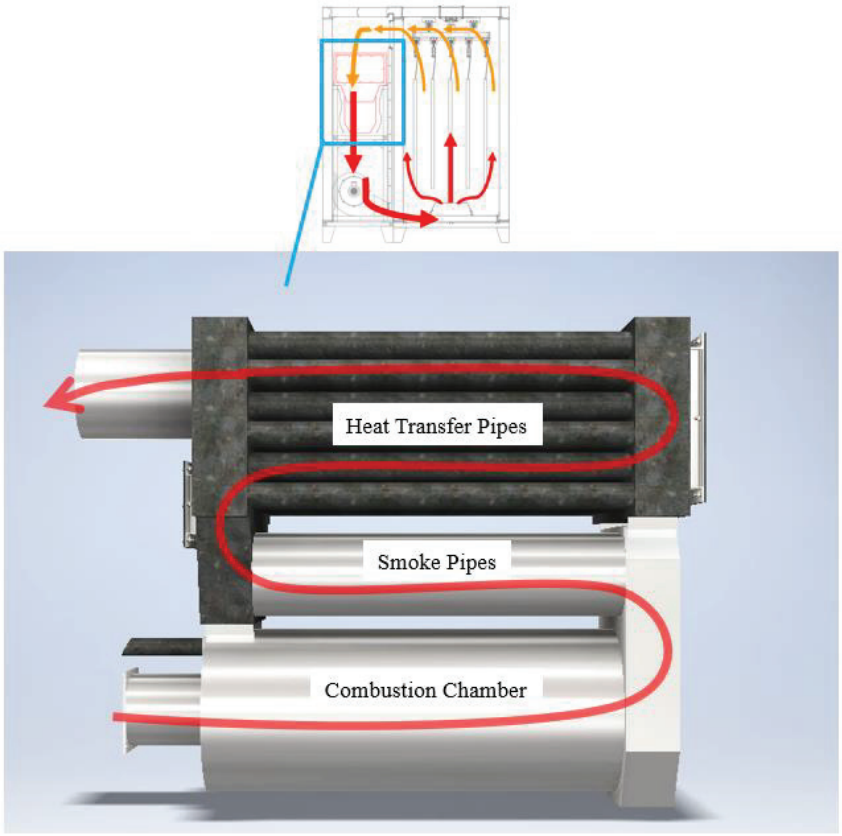

Figure 1.5. Sections of the Indirect Fired Heat Exchanger with hot gas flow path / ELECTRON Company Internal Report

Different heat exchanger designs are made according to the internal volume capacities of various ovens. Although the system is the same in general, some geometric parameters change. These parameters are pipe diameters and lengths. Approximately 56 pipes with various diameters and sizes are used in the heat exchanger. These pipes are joined to the turn sections by welding.

In the thermoblock, the outer fluid (cold) is the internal air of the oven, while the inner fluid (hot) produced by the burner is flue gas. The average temperatures of flue gas can vary between 1000°C and 850°C. Considering that the maximum temperature of the outer fluid (cold) used in this process is 200°C, the flue gas temperature in the chimney will be at least 200°C. When these values are considered, temperatures ranging from 1000°C to 200°C will occur on the heat exchanger surface. The heat exchanger with high temperatures tends to expand. It is foreseen that the expansion movement will be in one direction, and the heat exchanger design is made in this direction. However, due to non-homogeneous surface temperatures, expansion movements in different directions cause various stresses, which is the main reason for the plastic deformation of the heat

exchanger [5]. In addition, the high-temperature differences between the joined bodies are also a factor that increases the thermal stresses [6]. Because there are many rigidly mounted parts in the heat exchanger, each part shows a different expansion movement thanks to the thermal effects. The expansion movement causes a non-linear expansion situation.

Problems such as cracking, tearing, and rupture are observed in heat exchangers exposed to high thermal stresses. Figure 1.6. and Figure 1.7. show the cracking-tearing problems occurring at different points of the heat exchanger (especially around the combustion chamber). According to the information from the company, the relevant heat exchanger does not carry any extra load. The heat exchanger is mounted in the thermoblock only to carry its weight. For this reason, it is assumed that only the thermal stresses (occurring throughout the heat exchanger) cause plastic deformation, especially at the weakest points. Plastic deformation reduces the system's lifetime and efficiency. It is necessary to design a heat exchanger with a homogeneous temperature distribution to prevent plastic deformation.

Research has shown that there are several ways to distribute surface temperature homogeneously. One of them is orienting the external fluid flow uniformly to the heat exchanger, while the other is orienting homogeneous mass flow rates in the heat exchanger pipes. Gocmen *et al.* [7] documented that the external flow in a heat exchanger flow volume can have a normal mass flow rate distribution due to geometric improvements. Thus, homogeneous surface temperatures were obtained on the surfaces in contact with the external flow, reducing temperature differences. Cetkin *et al.* [8] documented numerically that homogeneous mass flow rate in the heat exchanger pipes can be obtained by cascading the inlet section of the heat exchanger, changing the pipe diameters, or orienting the flow directly to the pipes at the inlet. Academic studies show that a homogeneous mass flow rate distribution in pipes with the same alignment or dimension provides a homogeneous surface temperature distribution. In order to reduce the focus of the study, it is aimed to obtain homogeneous surface temperatures on the heat transfer pipes section of the heat exchanger (Figure 1.5.).

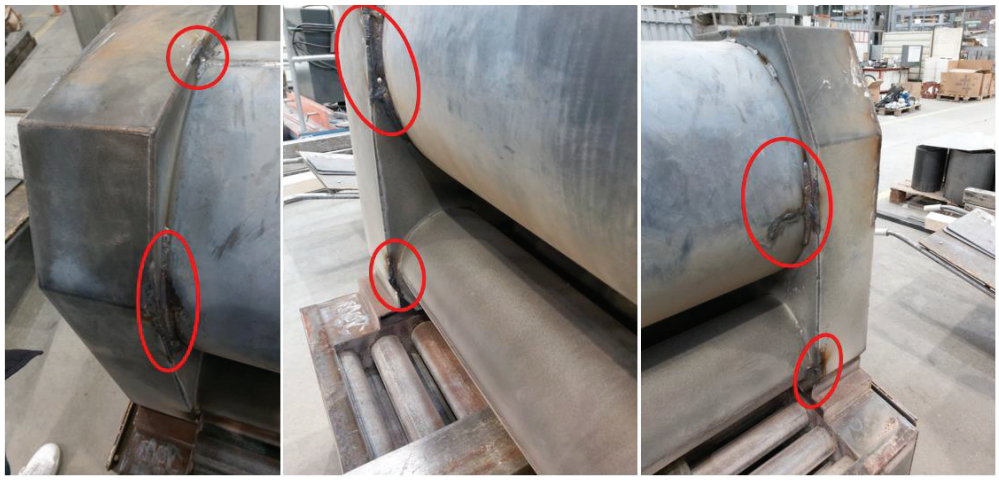

Figure 1.6. Some crack examples on the heat exchanger / ELECTRON Company Internal Report

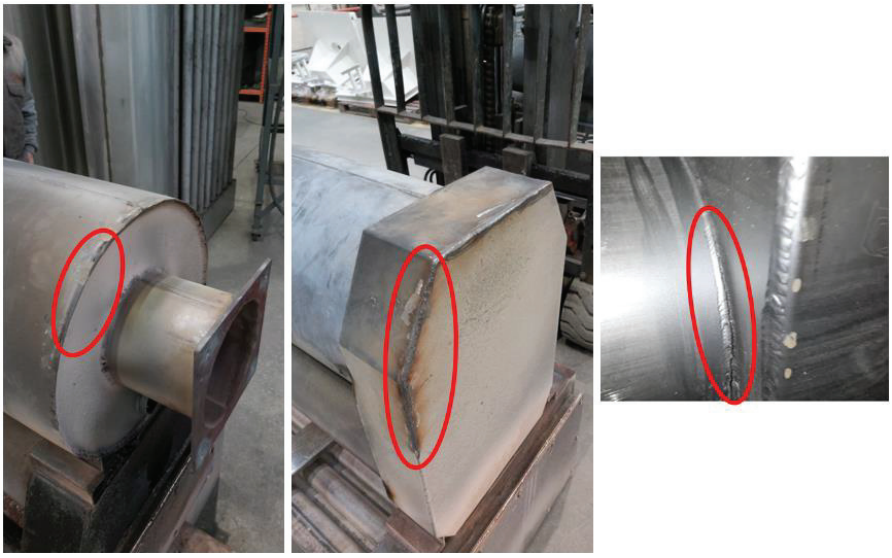

Figure 1.7. Some crack examples on the heat exchanger / ELECTRON Company Internal Report

The heat exchanger design that is the subject of the thesis will be provided from "ELECTRON / Sistem Teknik Makina San. Ve Tic. A.S.", which is the leader in the electrostatic powder coating sector in Turkey. To carry out the study, ELECTRON company shared the geometric data of the relevant heat exchanger, the material information, and the test results in some operating conditions.

First, the current-state will be analyzed, and then improvement studies will be carried out to obtain a homogeneous surface temperature distribution in the heat transfer pipes section.

CHAPTER 2

NUMERICAL MODEL

First, the current-state will be analyzed to document the temperature distribution and thermal stresses on the heat exchanger surface. This study's scope primarily focused on the heat transfer pipe section in the heat exchanger volume. Literature researches show that the homogeneously distributed surface temperatures are obtained in the heat transfer pipes where the pipe mass flow rates are homogeneously distributed (especially in cases where the external environment's temperatures are normally distributed) [7]. For this reason, firstly, the temperatures on the heat exchanger surface of the current state and the mass flow rates in the heat transfer pipes were documented. In the continuation of the study, the mass flow rate distribution in the heat transfer pipe section is homogenized.

2.1. Flow Volumes

To observe the state to be improved, the thermoblock region was chosen as the control volume. A convection drying oven of ELECTRON company was used as a model (Figure 2.1.). After the air (inside the oven) is sucked from the upper side of the thermoblock, it passes over the heat exchanger and is pressed to inside the oven again by the circulation fans (Figure 2.2.). In the current-state analysis, the effect of circulation fans will be ignored, and only the flow rates they provide will be used. For this reason, circulation fans are not included in the flow volume of the thermoblock. The flow volume is limited before the fan region. If the flow volume is examined in general; The internal air of the oven and the hot flue gases inside the heat exchanger are the flow volumes of the system.

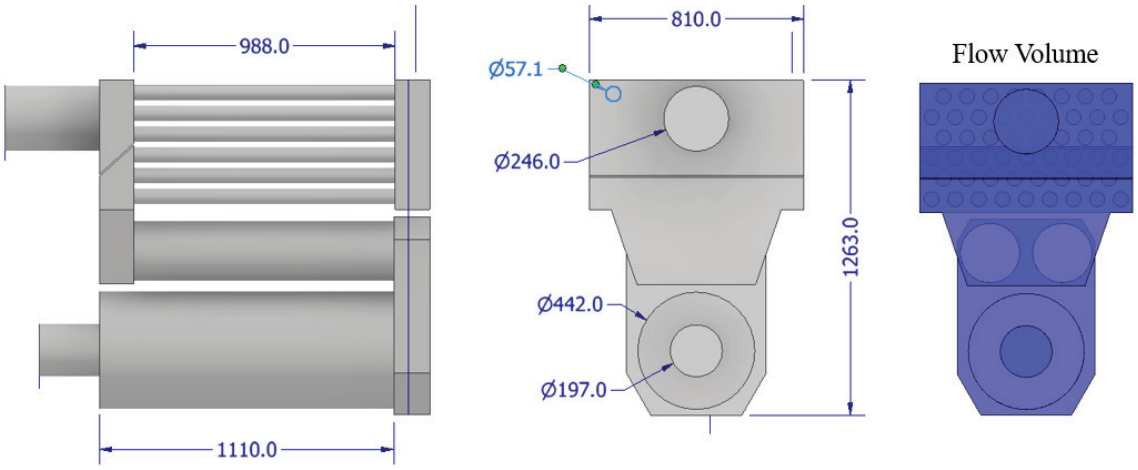

Figure 2.1. Dimensions of the Indirect-Fired Heat Exchanger flow volume (in mm) / ELECTRON Company Internal Report

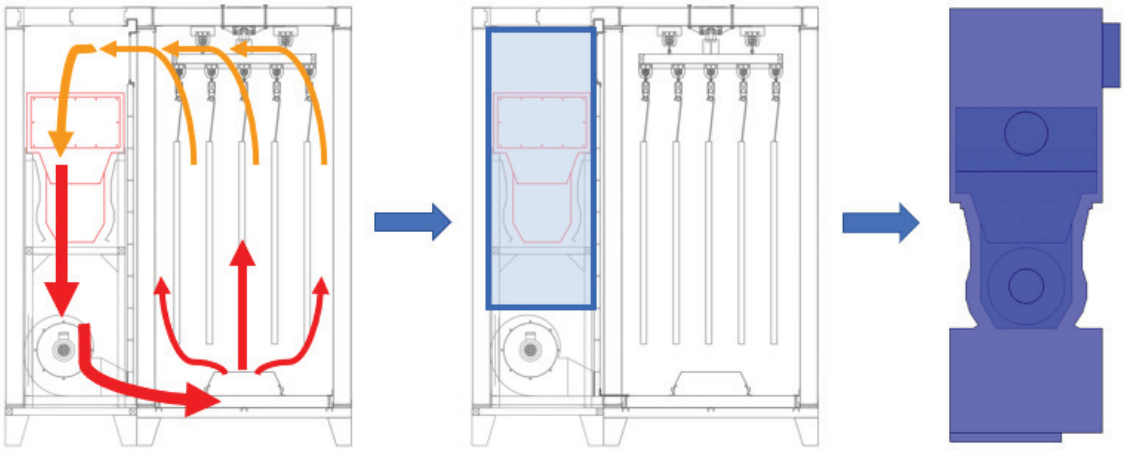

Figure 2.2. Extracting flow volume by considering external and internal flow in the thermoblock / ELECTRON Company Internal Report

It is the air circulating inside the oven. The heat source in the heat exchanger is the flue gases provided by the burner. In the current state, Natural Gas is used as the burner fuel. The quality and composition of the natural gas coming from the external environment to the burner are unknown. For this reason, the fluid in the heat exchanger is considered as air. Research shows that the thermophysical properties of flue gases [9] and air [10] converge considerably (Figure 2.3., Figure 2.4.). In addition, since the study will document the difference between the two cases, the assumption's effect will be minimal. Especially considering the temperature range that the fluids in the oven can have, air and flue gases have similar values in terms of thermophysical properties of that range.

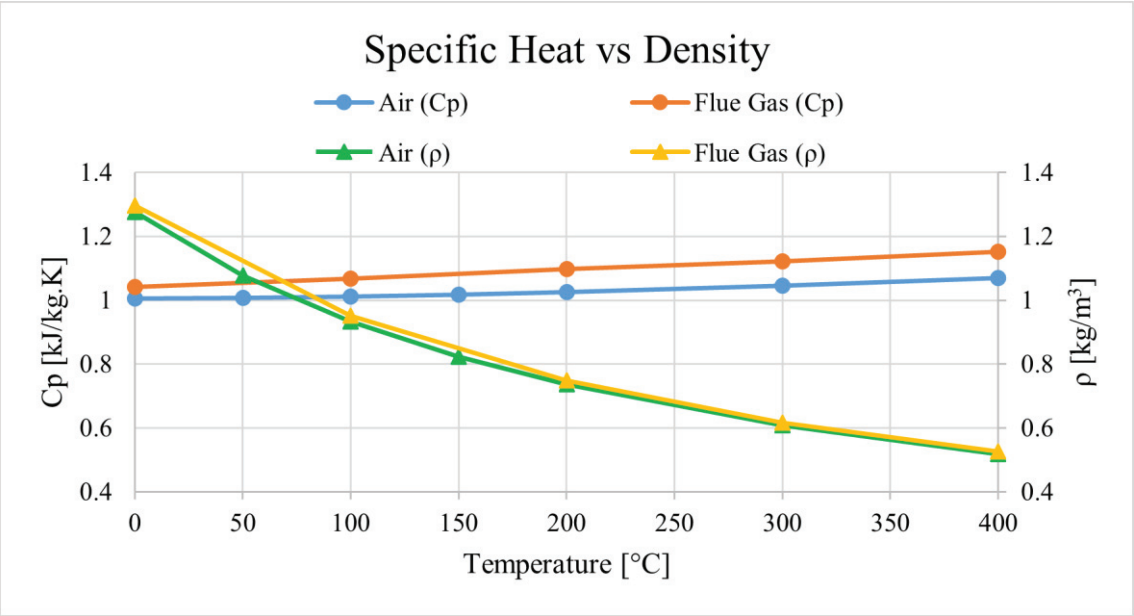

Figure 2.3. Comparison of flue gas and air for specific heat and density properties by temperature [9, 10]

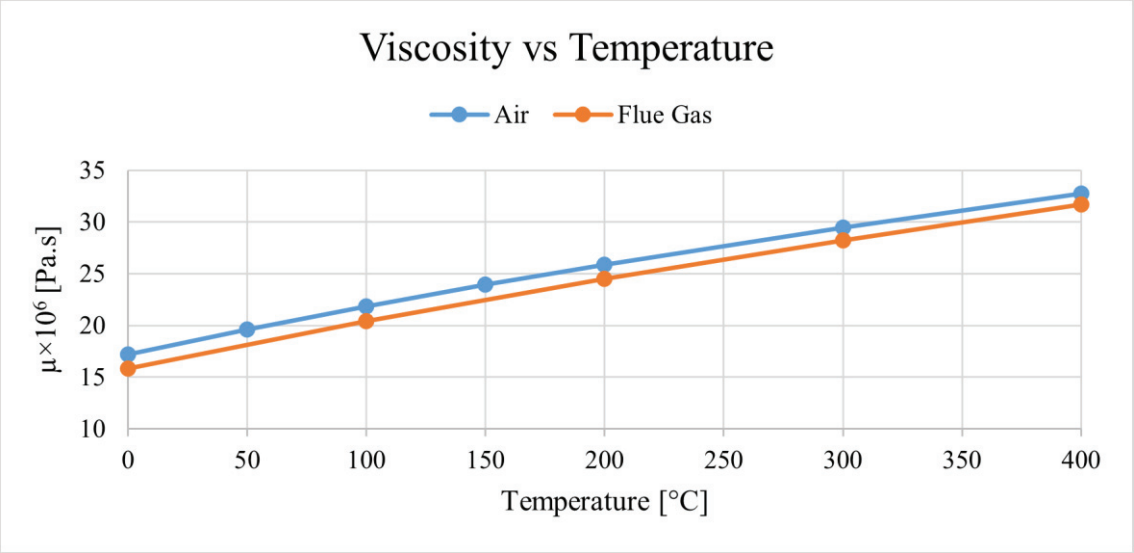

Figure 2.4. Comparison of flue gas and air for viscosity properties by temperature [9, 10]

2.2. Outer Walls

In the numerical model, it was tried to obtain the most straightforward geometry that best describes the acutal system as much as possible. For this reason, a solid body modeling between the flow volumes (between flow volumes or the external environment

of the control volume) has not been made. Instead, analytical calculations were made to provide the same thermal resistance, and the thermal resistance coefficients were defined on the surfaces. Since the volume of the thermoblock is the thermal source of the convection oven, the heat must be well preserved and not lost to the external environment. For insulation, the walls of the thermoblock have a sandwich structure. Galvanized metal material is used on the inside and outside parts of the wall layer. Stone wool material with high thermal resistance is used between these layers. Thus, the heat conduction is considerably reduced. Accordingly, the structure of the thermoblock wall is specified in Figure 2.5..

The thermal resistance of the wall structure [11], whose material properties are indicated in Table 2.1., was calculated as R_{wall} = 33.4 m^2.K/W (1). The thermal resistance is calculated per unit area. Since the R_{wall} will be defined to the related surfaces in the software, the area parameter will come from the related surfaces during the calculation.

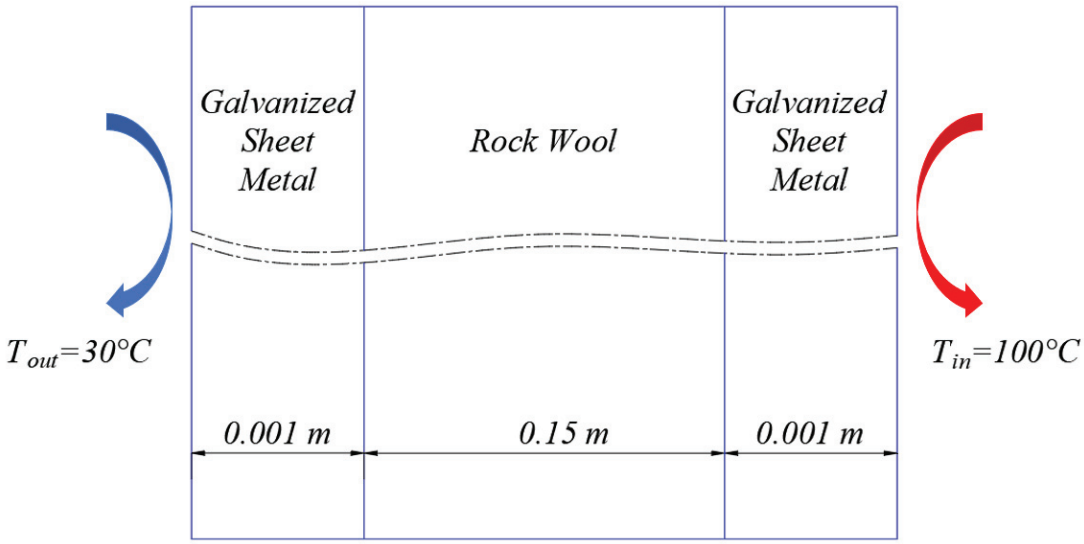

Figure 2.5. Cross-section view of the thermoblock's wall

$$\sum_{1}^{n} R_t = \frac{1}{h_{out} \times A_{Out}} + \frac{l_1}{k_1 \times A_1} + \frac{l_2}{k_2 \times A_2} + \cdots + \frac{l_n}{k_n \times A_n} + \frac{1}{h_{in} \times A_{In}} \qquad (1)$$

Table 2.1. Properties of thermoblock wall materials for thermal resistance calculation

Material	Thickness (m)	Heat Conduction Coefficient (k - W/m.K)	Heat Convection Coefficient (h – $W/m^2.K$)
Galvanized Sheet Metal [12]	0.001	16.27	-
Rock Wool [13]	0.15	0.045	-
Air @30°C [14]	-	-	20
Air @100°C [14]	-	-	200

Although different materials are used in the components, heat-resistant metal materials are generally used in the heat exchanger design. Since the study will document the difference between the two cases, the type and thickness of the material used in the heat exchanger are accepted as homogeneous. Especially since it is known that the heat is transferred in the heat transfer pipe section, the calculation of the thermal resistance over these pipes has increased the accuracy of the study. However, before separating the internal and external flows of the heat exchanger with a surface rather than a solid body, the definition of thermal resistance to be made on the heat exchanger surface must be validated.

2.3. Inner Walls (Surfaces)

Solid volumes were not modeled in this study to reduce the number of elements and shorten the analysis times. Instead, thermal resistances are defined for the surfaces where the fluid and solid are contacted. A comparison study provided the validation of this definition. A heat transfer pipe with a 3.2 mm thickness (Figure 2.6.) and its outer volume (Figure 2.7.) are considered for the validation study. Two models with the same conditions but different geometries were created for comparison. The first model separates the internal and external flow by the solid pipe volume (Figure 2.8.). The amount of heat transfer will be determined by the heat conduction coefficient of the solid material. In the second model, internal and external flows are separated by a surface (Figure 2.9.). The thermal resistance coefficient obtained from the analytical calculation is defined to this surface.

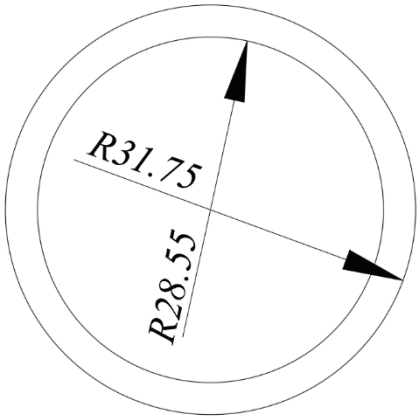

Figure 2.6. Dimensions (radius) of the heat transfer pipe (in mm)

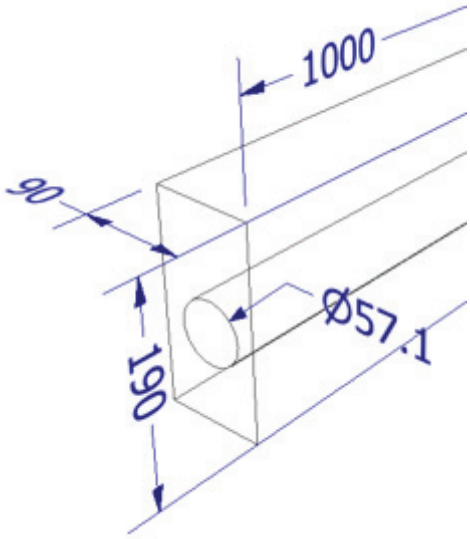

Figure 2.7. Dimensions of the outer volume of the heat transfer pipe thermal resistance validation cases

While r_{Inner} is 0.02855 m in heat transfer pipes, r_{Outer} is 0.03175 m (Figure 2.6.). It is the P236GH Non-alloy-steel that will be used throughout the analysis with the pipe material. The information of this material is given in Table 2.2..

Table 2.2. Thermal properties of P236GH Non-Alloy-Steel [15]

Material	Density [kg/m3]	Specific Heat [J/kg.K]	Thermal Conductivity [W/m.K]
P235GH	7900	470	49

In the validation study, where the solid pipe volume is not modeled, the contact thermal resistance to the pipe surfaces will be defined. The thermal resistance (R_t, $K.m^2/W$) of the pipe was calculated for a unit length (1 meter) using the 1-D heat conduction resistance equation [16].

$$R_t = \frac{\ln(\frac{r_{Outer}}{r_{Inner}})}{2 \times \pi \times k \times L} \quad (2)$$

The thermal resistance R_t on the contact surfaces was calculated as 3.45×10^{-4} $K.m^2/W$ (2). In order to perform a validation study, one of the heat transfer pipes was considered (in line with the current-state research analyses made before). Air at a temperature of 400°C with a mass flow of 0.0011 kg/s passes through the pipe selected in the research analysis. The outer volume of the relevant pipe is created rectangular to simulate the external flow movement in the current-state model. The external flow is perpendicular to the pipe surface (crossflow). The external flow rate and temperature are calculated from the current circulation fan flow rates and the average fluid temperature. The flow rate of the fluid which is perpendicular to a heat transfer pipe's surface, was determined as approximately 0.4 kg/s, while the fluid temperature was determined as 50°C. With these boundary conditions, both with and without pipe (solid) flow volumes were analyzed, and the exit air's average temperature was calculated. Since the boundary conditions are the same in the study, the critical factor is the validity of the thermal resistance assumption.

Reynolds numbers were calculated for inner and outer flows to see any turbulence effects in the flow volumes. The cross-section area where the outer flow enters the flow volume is 0.09 m width and 1 m length (Figure 2.7.). In the external flow, the flow passes at a mass flow rate of 0.4 kg/s at 50°C. The hydraulic diameter of the external flow is calculated as 0.165 m [17]. A mass flow rate of 0.0011 kg/s passes through the inner flow volume at 400°C. The hydraulic diameter of the inner flow is known as 0.0571 m. The Reynolds Number [18] of the inner flow is 754.7 while the outer flow is 37,580.4 [19] [20], respectively.

$$Re = \frac{\rho \times V_{Avg} \times D_h}{\mu} \quad (3)$$

$$D_h = \frac{4 \times w \times L}{2 \times (w + L)} \tag{4}$$

Due to the high Reynolds number in the external flow, the RANS k-Epsilon (realizable) turbulence model was used in the related study. The literature has verified that realizable k-Epsilon is converged well both in and out of pipe flows [21].

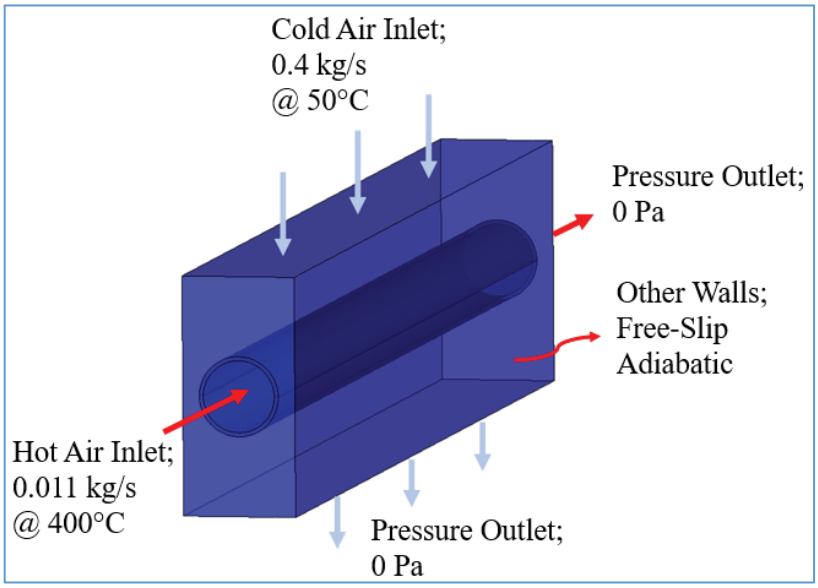

Figure 2.8. Thermal resistance validation model – with pipe

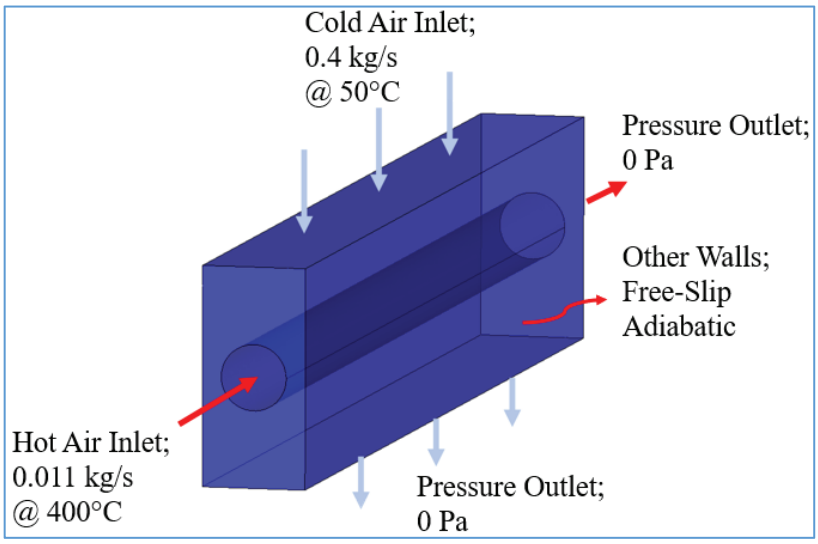

Figure 2.9. Thermal resistance validation model – without pipe

Thermal resistance validation analyses were performed in a time-independent approach (steady-state). The comparison between the two cases is based on the average temperature of the outer flow as it leaves the system (Figure 2.10.). Temperature values were read from the outlet surface using the "area-weighted average" calculation method. Outer fluid entering the flow volume at a temperature of 50°C; In the case where the pipe is modeled as a solid volume, the outer fluid leaves the system at 57.11 °C, while in the pipeless case where the thermal resistance is defined to the contact surfaces, it leaves the system as 56.93 °C. Due to the outer fluid's average outlet temperature is very close in the cases, defining the thermal resistance to the contact surfaces without pipe volumes will preserve the accuracy of the studies. In addition, the computational cost of the analyzes (maximum element quantity, element quality, calculation time) is reduced.

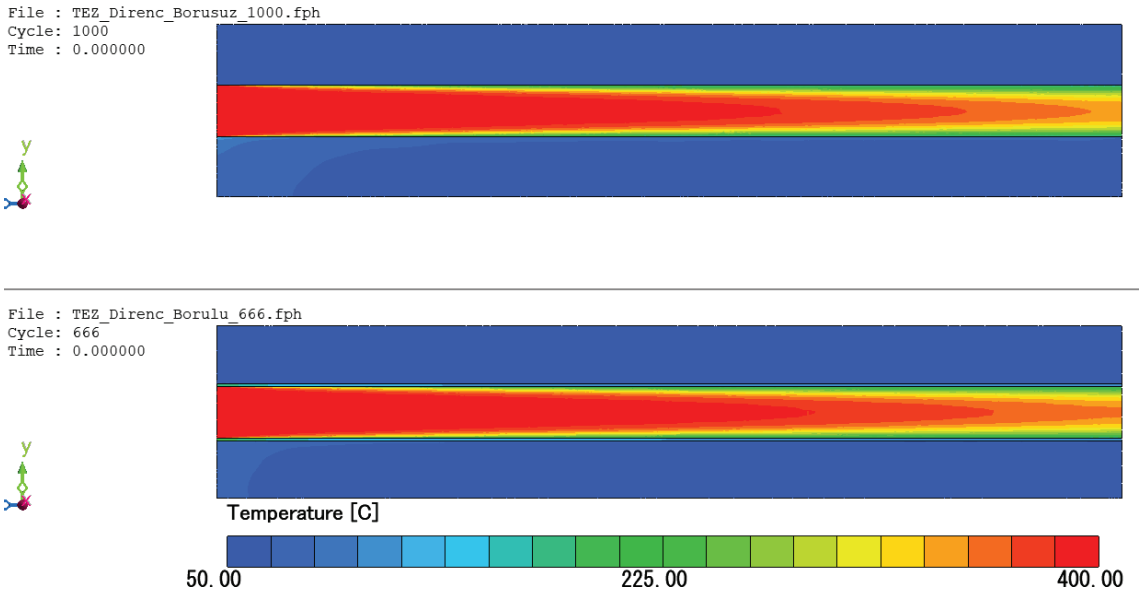

Figure 2.10. Temperature contours where the external flow is in the -y direction; the top is "without pipe", and the bottom is "with pipe"

2.4. Conditions

2.4.1. Hot Gas Inlet

Energy and flow equations will be used to analyze the numerical model. The ELECTRON company provided measurement data to determine the system's boundary

conditions. A natural gas-fuel burner is used in the convection oven. The instantaneous gas flow rate consumed by the burner is uncertain, but the flow rate of the chimney gases at the outlet can be measured. Chimney gases are polluted and therefore contain various particles. For this reason, the measurement of gases is provided by a differential pressure transmitter instead of an anemometer. With the differential pressure transmitter, the pressure difference is measured at various points from the edge of the chimney duct to the center point (Figure 2.11.).

Figure 2.11. Measurement of the pressure differences of the chimney gas to obtain volume flow rate of it

The average pressure difference is measured as 14.8 Pa, and also the temperature is measured as 102.2 °C of the chimney gas. The fluid density calculation formula by the constant coefficient of the pitot tube used for the measurement is specified by the supplier company (5). The average flow velocity in the chimney was calculated using the Bernoulli equation (7). During the measurements made in the chimney, the height from the ground is 10 meters.

$$\rho = \frac{336.75}{T_{Gas} + 273.15}\ [kg/m^3] \quad (5)$$

$$P + \frac{1}{2} \times \rho \times V^2 + \rho \times g \times h_L = Const. \quad (6)$$

$$V_{Gas} = \sqrt{\frac{2 \times \Delta P}{\rho}}\ [m/s] \quad (7)$$

$$\dot{V} = V_{Gas} \times A_{Chimney}\ [m^3/s] \quad (8)$$

$$\dot{m} = \dot{V} \times \rho\ [kg/s] \quad (9)$$

When the data is used in the relevant equations, the gas flow rate in the chimney is determined as 0.253 kg/s where the $D_{Chimney}$ is 0.25 m, so $A_{Chimney}$ is 0.05 m^2.

Since the temperature of the gas provided by the burner is relatively high, it could not be measured with a thermocouple. Also, the heat exchanger is in a hard-to-reach location (inside the thermoblock), the measurement could not be taken with a thermal camera. Therefore, combustion analysis measurements were performed at the outlet of the heat exchanger by the company. These measurements were performed at the various chimney and oven temperatures. The efficiency of combustion in the burner and the amount of air used are obtained by the measurements. The measurement, which is the subject of the thesis, is the measurement of the situation where the temperature inside the oven is 50°C, and the average chimney gas temperature is 270°C (Table 2.3.).

Table 2.3. Real-time experimental measurements of the oven by ELECTRON Company

Temperature Inside the Oven [°C]	Chimney Gases Temperature [°C]	Ref. Air Temperature [°C]	λ	Excess Air [%]	Combustion Efficiency (Calculation) [%]
50	270	20	1.78	78	92.38

As a result of an ideal combustion reaction, the lambda (λ) value is desired to be 1 [22]. The excess air ratio calculated at the end of combustion is added to the lambda value. It is observed that there is 78% excess air in the lambda value in the current measurement (Table 2.3.). In the previous chimney gas measurement, the instantaneous air density was calculated as 0.897 kg/m^3 (5). From here, the chimney gas mass and volume flow rates are calculated as 0.253 kg/s and 0.282 m^3/s at the outlet (10). If the excess air rate in the flue gas is 78%, the actual combustion gases (air + natural gas) rate is 22%. The total volumetric flow rate of the actual combustion gases is calculated as 0.06204 m^3/s (Table 2.5.). According to literature, 8.66 m^3 of air is used to burn 1 m^3 of natural gas (Table 2.4.) [23]. In other words, if we consider the volume of combustion gases as 9.66 m^3, 10.4% of this mixture is natural gas (fuel), and 89.6% is air. In that case, the fuel (natural gas) flow rate in the chimney gas is 0.006422 m^3/s (Table 2.5.). Since the heating value of natural gas is 10 kWh/m^3 [23], the heat inlet by the natural gas to the system is calculated as 231.2 kJ/s by unit time (1 hour = 3600 seconds) (14). The required air for the combustion is sucked from the outside. When the ambient temperature is 25°C, the enthalpy of the air is 298.18 kJ/kg [24]. The energy of the air (89.6% of the combustion gases energy) in the combustion gases is determined as 67.63 kJ/s. The total heat input is approximately 299 kJ/s by considering the heat inputs from natural gas and air. Since the total output mass flow rate was previously measured (calculated) as 0.253 kg/s at the chimney, the hot fluid enthalpy is finally calculated as 1184.28 kJ/kg. Since the fluid in the heat exchanger is considered as air, the air temperature corresponding to this energy is approximately 850°C (Table 2.6.) [24].

Finally, the hot air inlet is defined as the heat exchanger hot gas inlet at a mass flow rate of 0.253 kg/s and a temperature of 850°C.

Table 2.4. Some thermophysical properties of Natural Gas [23]

Properties	Values
Heating Value	10 kWh/m^3
Minimum Air Requirement (Ratio)	8.66
Minimum O2 Requirement (Ratio)	1.82

$$\rho = \frac{\dot{m}}{\dot{V}} \tag{10}$$

$$\dot{V}_{Chimney} = \dot{V}_{Excess\ Air} + \dot{V}_{Combustion\ Gases} \quad (11)$$

$$\dot{V}_{Combustion\ Gases} = \dot{V}_{Air} + \dot{V}_{Natural\ Gas} \quad (12)$$

Table 2.5. Determination of the volumetric flow rate of the Natural Gas in the combustion gases

	Variable	Value
Chimney Gases	Measured Density of the Chimney Gases (10)	0.897 kg/m^3
	Mass Flow Rate of the Chimney Gases	0.253 kg/s
	Volumetric Flow Rate of the Chimney Gases (11)	0.282 m^3/s
	Excess Air Rate in the Chimney Gases	78%
	Combustion Gases Rate in the Chimney Gases	22%
	Volumetric Flow Rate of the Combustion Gases in the Chimney Gases (12)	0.06204 m^3/s
Combustion Gases	Min. Air Requirement to Burn 1 m^3 of Natural Gas [23]	8.66 m^3
	Relative Ratio of the Natural Gas in the Combustion Gases	10.4%
	Volumetric Flow Rate of the Natural Gas in the Combustion Gases	0.006422 m^3/s

$$\dot{m}_{Chimney\ Gases} \times h_{Chimney\ Gases} = (\dot{m}_{Air} \times h_{Air}) \times \dot{Q}_{Natural\ Gas} \quad (13)$$

$$\dot{Q}_{Natural\ Gas}\left[\frac{kJ}{s}\right] = 10\left[\frac{kW \times 3600[s]}{m^3}\right] * 0.006422\ [\frac{m^3}{s}] \quad (14)$$

Table 2.6. Determination of the temperature of hot gas inlet to the heat exchanger

Variable	Value
Heat Flow Rate of the Natural Gas (14)	231.2 kJ/s
Mass Flow Rate of the Air @25°C (89.6% of the Combustion Gases)	0.227 kg/s
Enthalpy of the Air @25°C	298.18 kJ/kg
Mass Flow Rate of the Chimney Gases (13)	0.253 kg/s
Enthalpy of the Chimney Gases	1184.28 kJ/kg
Temperature of the Hot Gas Inlet [24]	1120 K ~ 850°C

2.5. Setup Properties

The openings in the system are defined as the surfaces opening to the atmosphere where the backpressure is 0 Pa. Gas entry into the heat exchanger is 0.253 kg/s. The same turbulence model continued to be used due to the high Reynolds numbers as calculated in the thermal resistance validation study. Since the study was concerned with the state data where the system was stable, the analysis was carried out in a steady-state, time-independent manner. As the convergence criterion, it is aimed to decrease the relative fluctuations below 10^{-6}.

In order to observe the radiation effects, analyzes were carried out with or without the radiation equations included in the numerical solution.

The mesh dependency test was carried out for the heat exchanger's flow volume (which is the study's main subject) to observe the effect of the mesh structure on the results. According to the results, the mesh structure was selected with the least number of elements and the accrued result.

2.5.1. Current State of the Model

Since there is no previous study on the current model, the current situation was first analyzed, and the temperature distribution on the heat exchanger surface was observed. In this study, since it is argued that the homogeneous flow rate distribution in

the heat transfer pipes will provide the homogeneous surface temperatures, the flow rates in the pipes have also been read. In order to read the mass flow rates in the pipes correctly, the necessary reading process must be made after a uniform flow region is developed. For this reason, the flow rates were read from the outlet surfaces of the heat transfer pipe section.

A naming procedure has been developed to read the data. The naming procedure for each pipe is "D#(Turn SectionName)_#(LineNumber)#(ColumnNumber)" and the current direction of flow is considered while sorting (Figure 2.12.). For example, in "D1_12" code, "D1" means 1st turn, and the "12" means 1st line and 2nd column. Or in "D2_21" code, "D2" means 2nd turn while the "21" means 2nd line and 1st column (Figure 2.13).

For the current-state, all heat transfer pipes have the same diameter. The inner pipe diameter of the pipes is Ø57.1 mm.

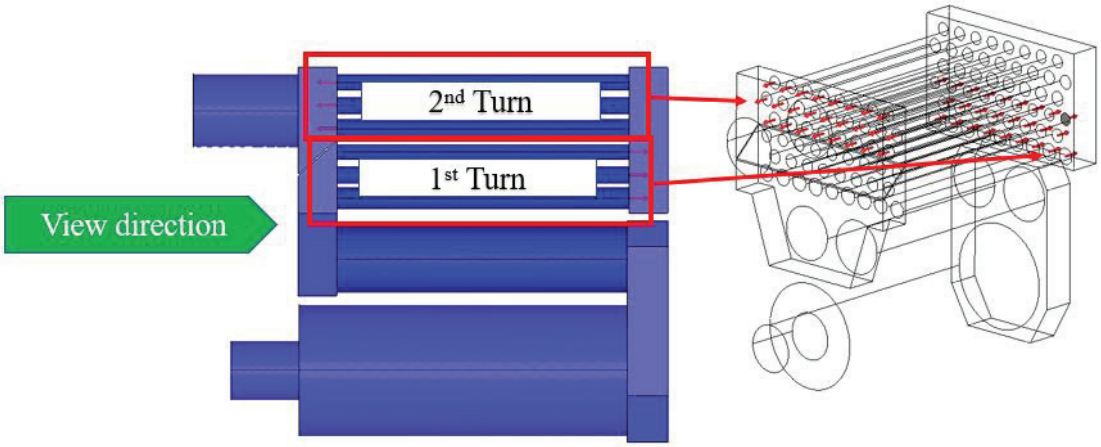

Figure 2.12. View direction for naming codes and flow directions in the turn sections of the heat transfer pipes

	9	8	7	6	5	4	3	2	1	
TURN-2		d2_38	d2_37	d2_36	d2_35	d2_34	d2_33	d2_32	d2_31	3
	d2_29	d2_28	d2_27	d2_26	d2_25	d2_24	d2_23	d2_22	d2_21	2
		d2_18	d2_17	d2_16	d2_15	d2_14	d2_13	d2_12	d2_11	1
TURN-1	d1_31	d1_32	d1_33	d1_34	d1_35	d1_36	d1_37	d1_38	d1_39	3
		d1_21	d1_22	d1_23	d1_24	d1_25	d1_26	d1_27	d1_28	2
	d1_11	d1_12	d1_13	d1_14	d1_15	d1_16	d1_17	d1_18	d1_19	1
	1	2	3	4	5	6	7	8	9	

Figure 2.13. Cross-section numbering of the pipes due to flow and view direction of "Figure 2.12."

The flow volumes in the thermoblock are created without solid parts. Extending the surfaces where the flow enters ensures that the flow enters the system with a uniformly distributed velocity profile. As mentioned before, the fans in the thermoblock are not included in the flow volume.

Three different views of the flow volumes are shown in Figure 2.14. and Figure 2.15.. As seen in Figure 2.14., the flow volumes are separated by surfaces. While the hot air enters the “HEX inlet”, the cold air enters from the “Thermoblock inlet”. Control volume of the heat exchanger and outer side of it are shown in Figure 2.16., Figure 2.17., and Figure 2.18..

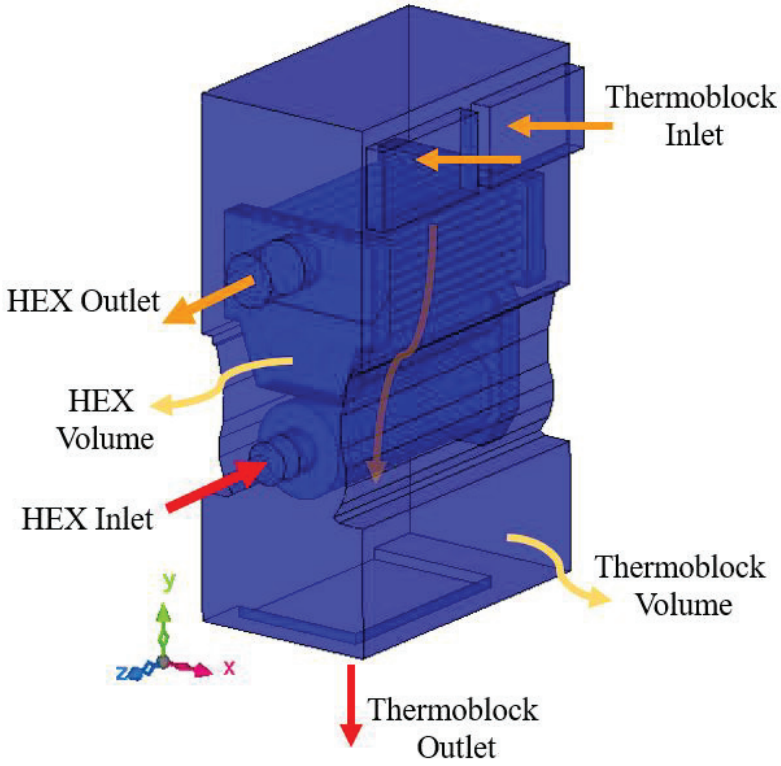

Figure 2.14. Flow volumes and flow directions of the current-state case (Cross view)

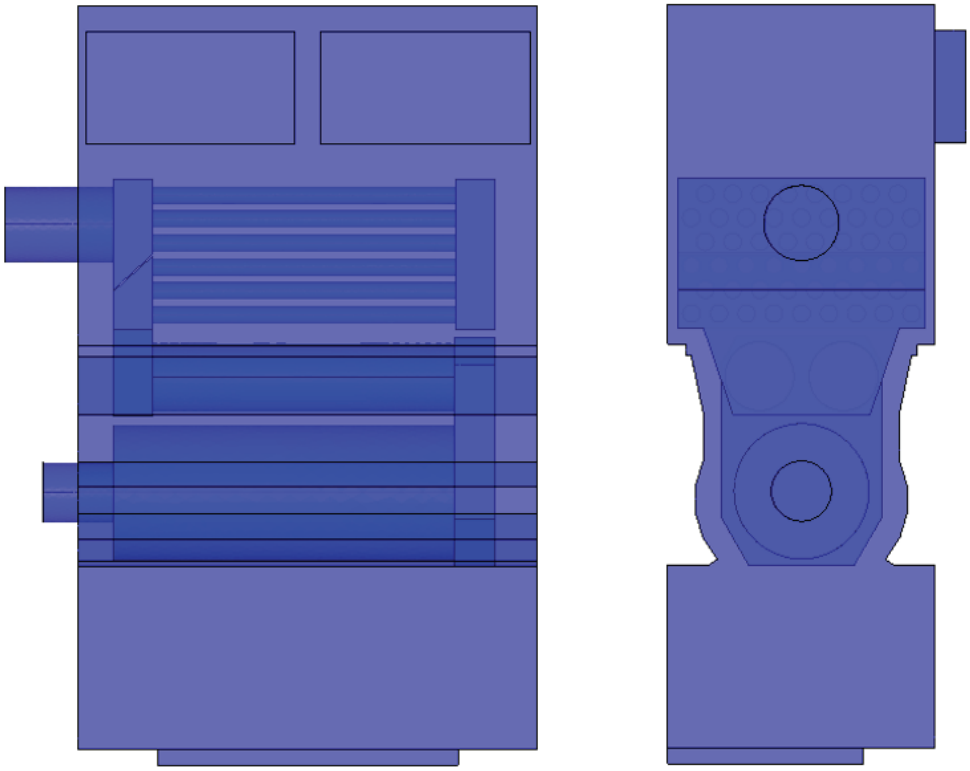

Figure 2.15. Control volumes of the thermoblock component – Front and side view

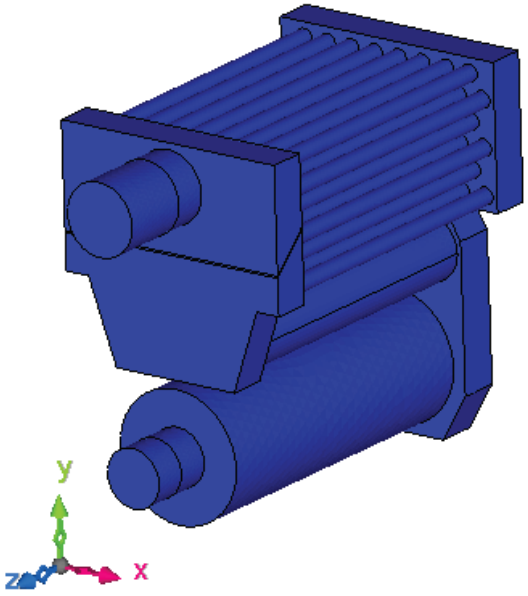

Figure 2.16. Control volume of the Indirect Fired Drum & Tube Heat Exchanger – Cross view

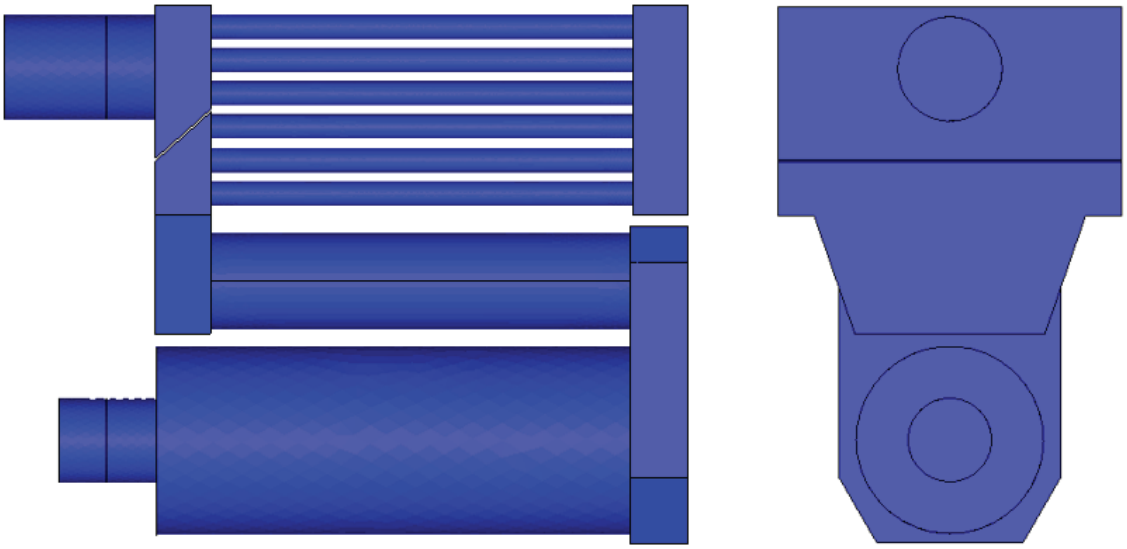

Figure 2.17. Control volume of the Indirect-Fired Drum & Tube Heat Exchanger – Front and Side views

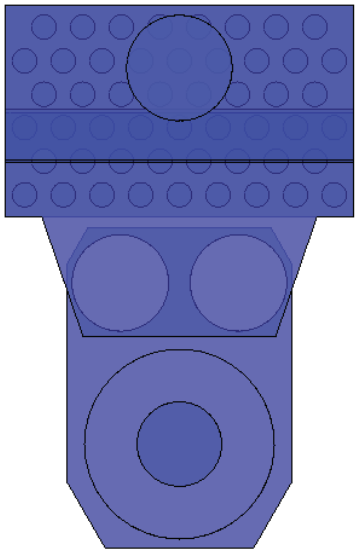

Figure 2.18. Transparent side views of the Indirect-Fired Drum & Tube Heat Exchanger flow volume

Cross, front and side views of the outer flow volume of the heat exchanger are shown in Figure 2.19. and Figure 2.20..

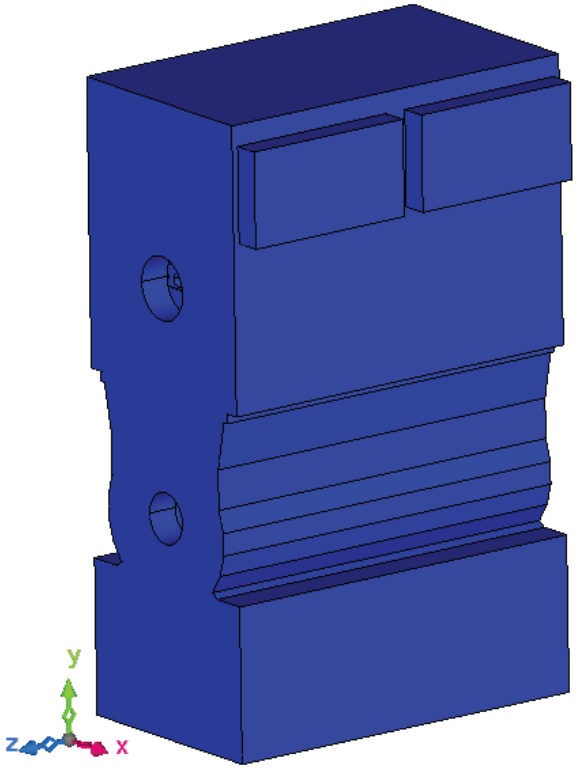

Figure 2.19. Outer flow volume of the heat exchanger – Cross view

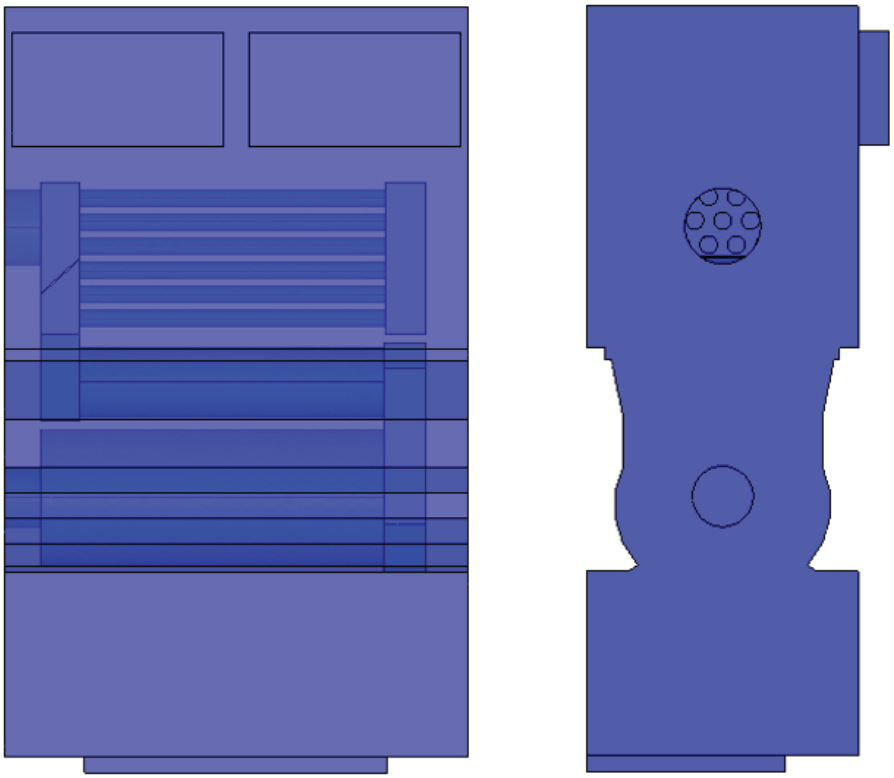

Figure 2.20. Outer flow volume of the heat exchanger – Front and side view

After defining the flow volumes, the naming procedure is done on various surfaces to define the boundary conditions. The inlet and outlet parts of the heat exchanger are defined as “hex_inlet” and “hex_outlet” in Figure 2.21..

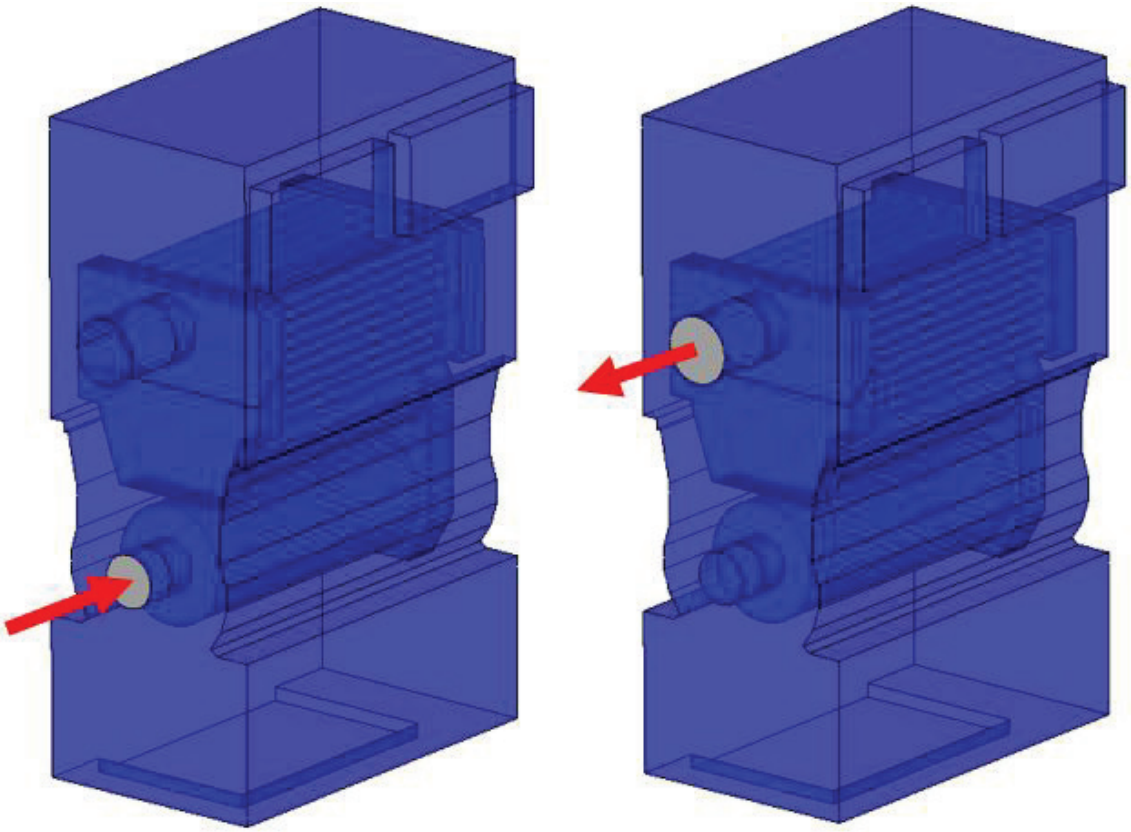

Figure 2.21. “Hex_inlet” (left) and “hex_outlet” (right) named selections and flow directions of the Heat Exchanger flow volume

The surfaces between heat exchanger (inner) flow volume and thermoblock (outer) flow volume are named as “wall_hex” (Figure 2.22.). The walls of the outer flow volume in contact with the ambient environment are named as “wall_thermo” (Figure 2.22.).

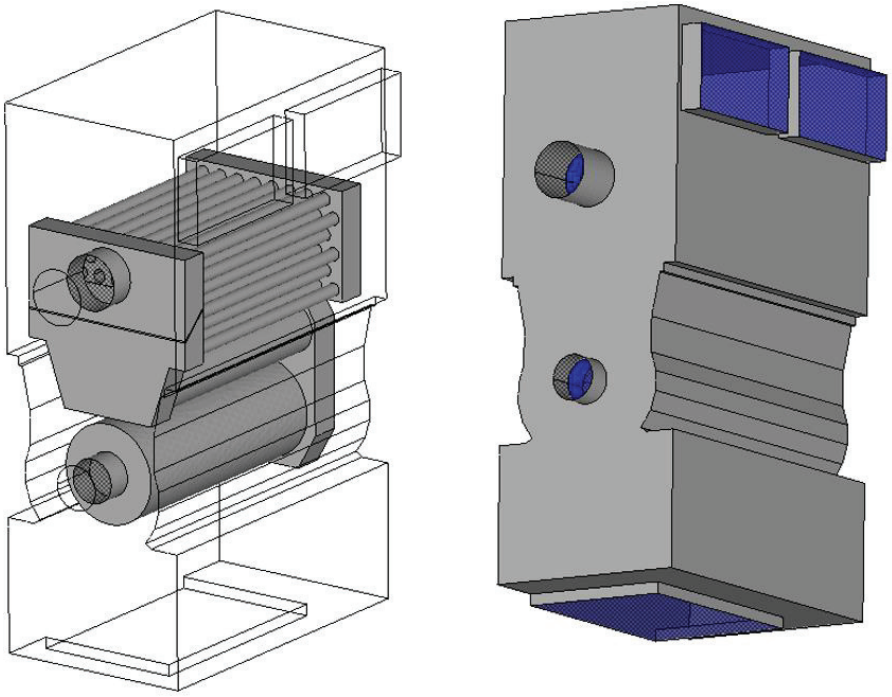

Figure 2.22. “Wall_hex” (left) and “wall_thermo” (right) named selections of the heat exchanger and thermoblock flow volumes

External flow’s inlet and outlet surfaces (which is sucked from inside of the oven) are named as “thermo_inlet” and “thermo_outlet” in Figure 2.23..

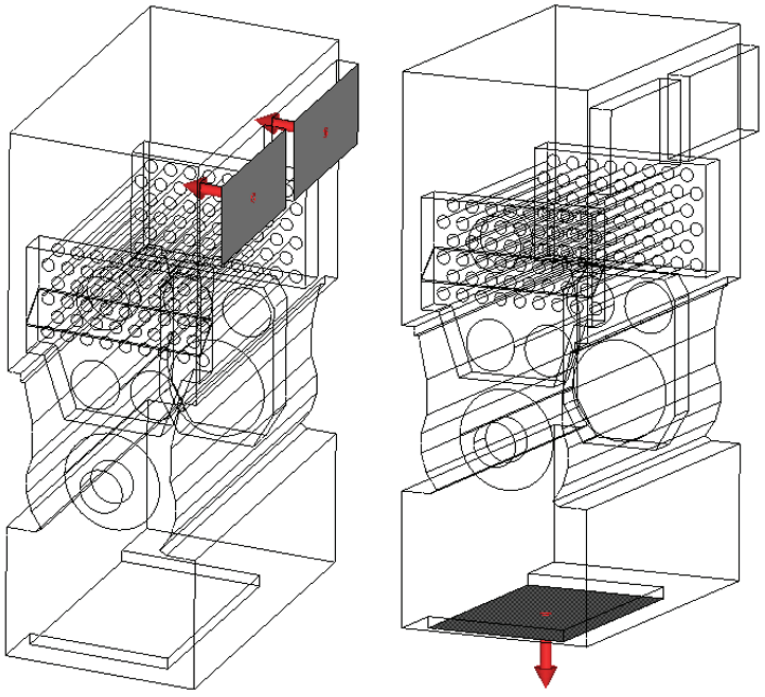

Figure 2.23. “Thermo_inlet” (left) and “thermo_outlet” (right) named selections and flow directions of the thermoblock flow volume

Boundary conditions defined for the current-state analysis are in Table 2.7.. Since this study aims to see the effect of the optimization changes on thermal stresses, the boundary conditions were kept the same during the study.

Table 2.7. Analysis conditions

Named Selection	Condition
Hex_inlet	0.253 Kg/s mass flow rate – Air @ 850°C
Hex_outlet	0 Pa Static Pressure (Outflow)
Wall_hex	0.000345 $K.m^2/W$ Thermal resistance with No-Slip (2)
Thermo_inlet	2.8 Kg/s mass flow rate – Air @ 50°C
Thermo_outlet	0 Pa Static Pressure (Outflow)
Wall_thermo	33.4 $K.m^2/W$ Thermal resistance with No-Slip (1)

Although there are high temperatures in the flow volumes, it is difficult to see the radiation effects clearly because there are no solid parts. Current-state analysis was performed with radiation equations (VF method) and without radiation equations to validate this. Since there was no significant difference in surface and outlet temperatures between these two analyses, the radiation effect was not considered to reduce the computational cost.

Because of the no element quality problem and providing a more accurate solution with fewer elements due to its many faces, Polyhedral mesh is used in the analysis [25]. The CFD software first creates the hexahedral elements (Figure 2.24.) to predict the mesh sensitivity and allow arrangement (refine, merge).

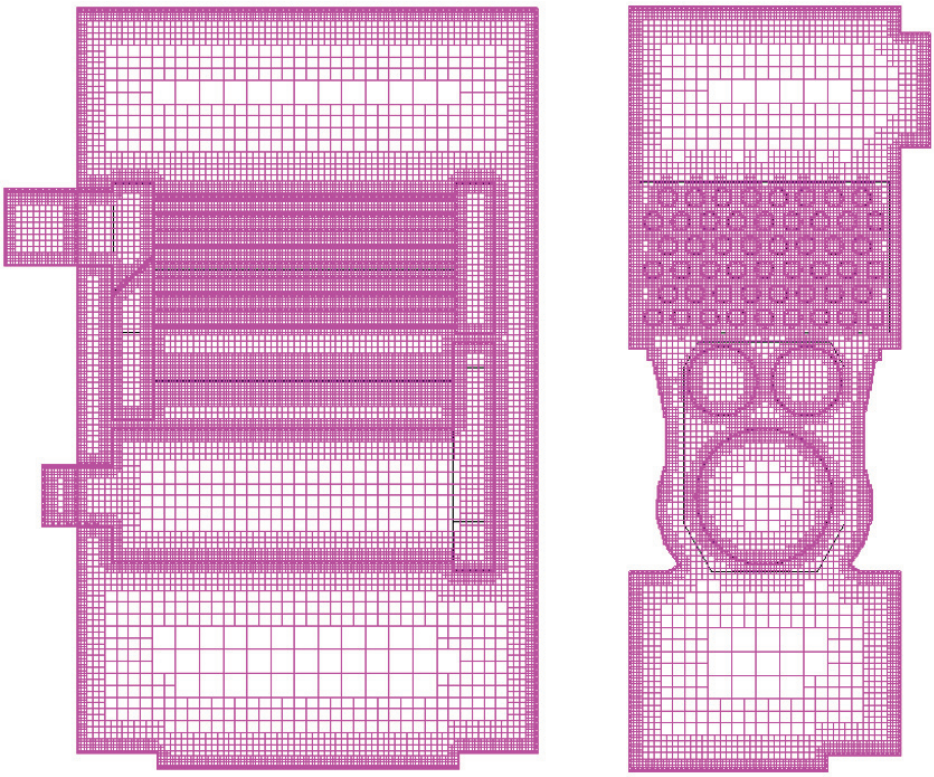

Figure 2.24. Hexahedral meshed flow volumes (Front and side view)

At the end of the meshing process, all elements were transformed into a Polyhedral mesh (Figure 2.25.). The total number of elements is 9,234,158, and the boundaries have three layers (Figure 2.26.).

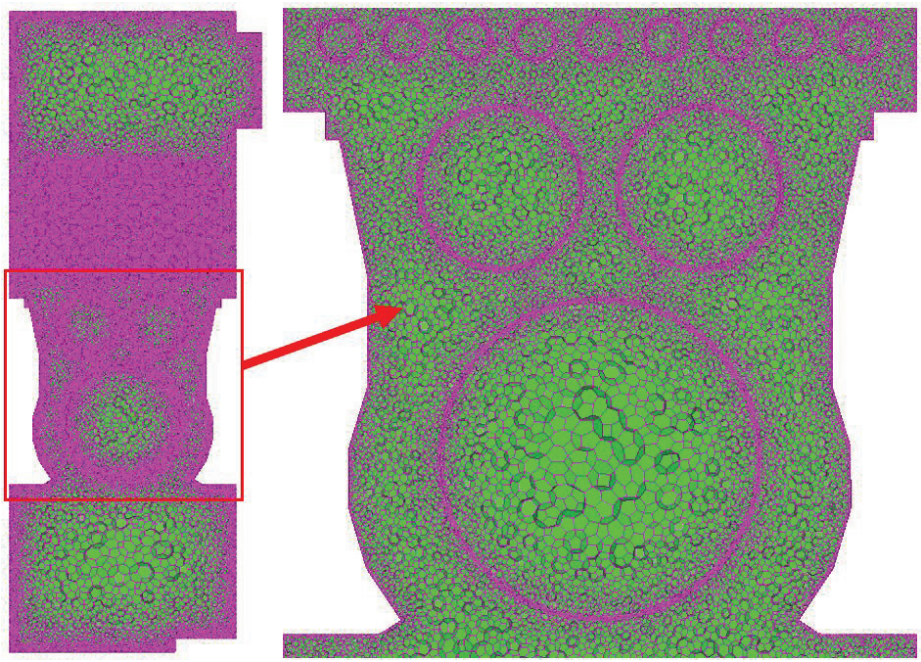

Figure 2.25. Polyhedral mesh conversion of the flow volumes with boundary layers

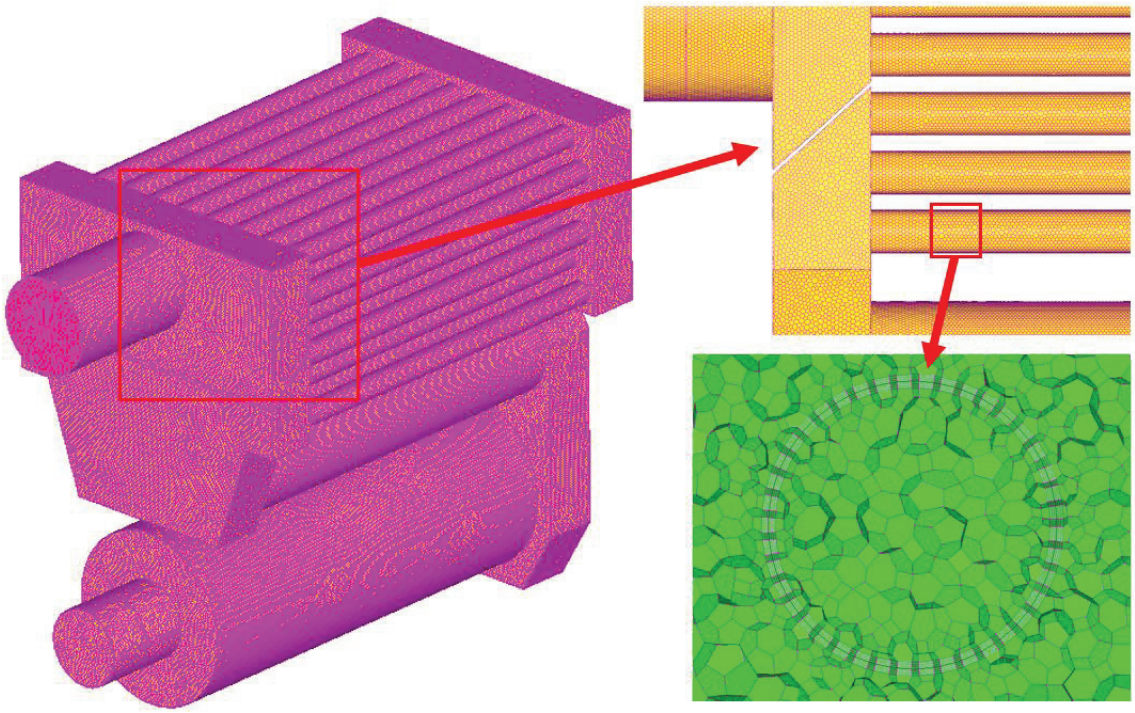

Figure 2.26. Boundary layers of the Polyhedral mesh in the pipe sections

2.5.2. Outputs of the Current-State Model

The convergence criteria of the analysis was determined as 10^{-5} relative fluctuation of the residuals. After achieving this relative error difference, it was solved and stopped at the 1000th iteration (Figure 2.27.).

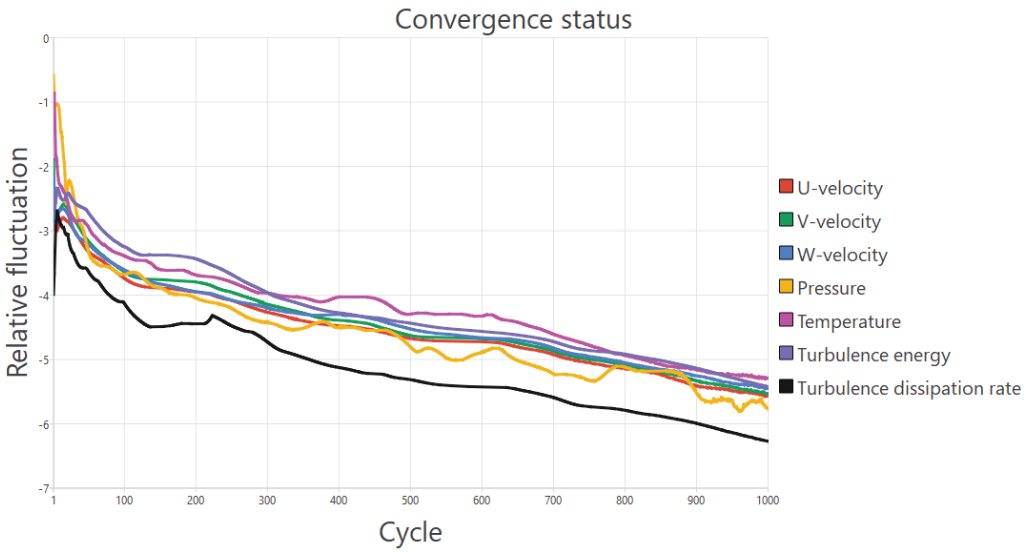

Figure 2.27. Convergence graph of the current-state analysis

As a result of the analysis, the temperature and pressure difference values observed at the inlet and outlet of the heat exchanger and thermoblock volumes are given in Table 2.8.. Especially the fluid temperature at the heat exchanger outlet is quite close to the Table 2.3. data.

Table 2.8. Outputs of the current-state model

Condition	Output
HEX Inlet Temperature	850 °C
HEX Outlet Temperature	280.7 °C
Thermoblock Inlet Temperature	50 °C
Thermoblock Outlet Temperature	98 °C
Pressure Difference in HEX (ΔP)	57.7 Pa

The temperature counters resulting from the analysis were first monitored visually (Figure 2.28.). As seen in the outlet region of the external flow, the temperature of the fluid entering the thermoblock (cold air) has increased. The hot air temperature entering the heat exchanger has decreased on the heat exchanger side.

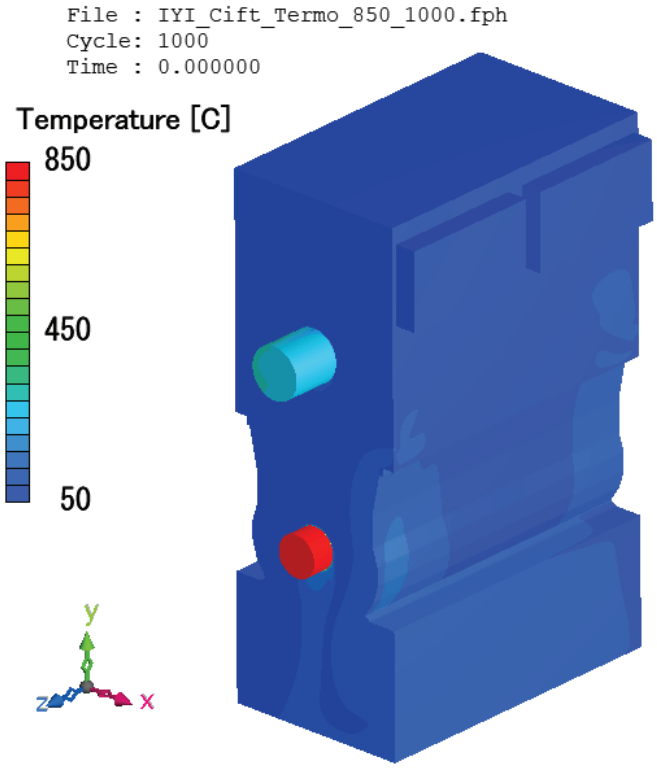

Figure 2.28. Temperature counters of outer surfaces

The temperatures of the inner and outer flows were monitored in different turn sections (Figure 2.29.). As it is seen, there are different flow temperatures in the heat transfer pipes sections (Turn-1 & Turn-2). There is also a sharp transition (differences) between temperatures.

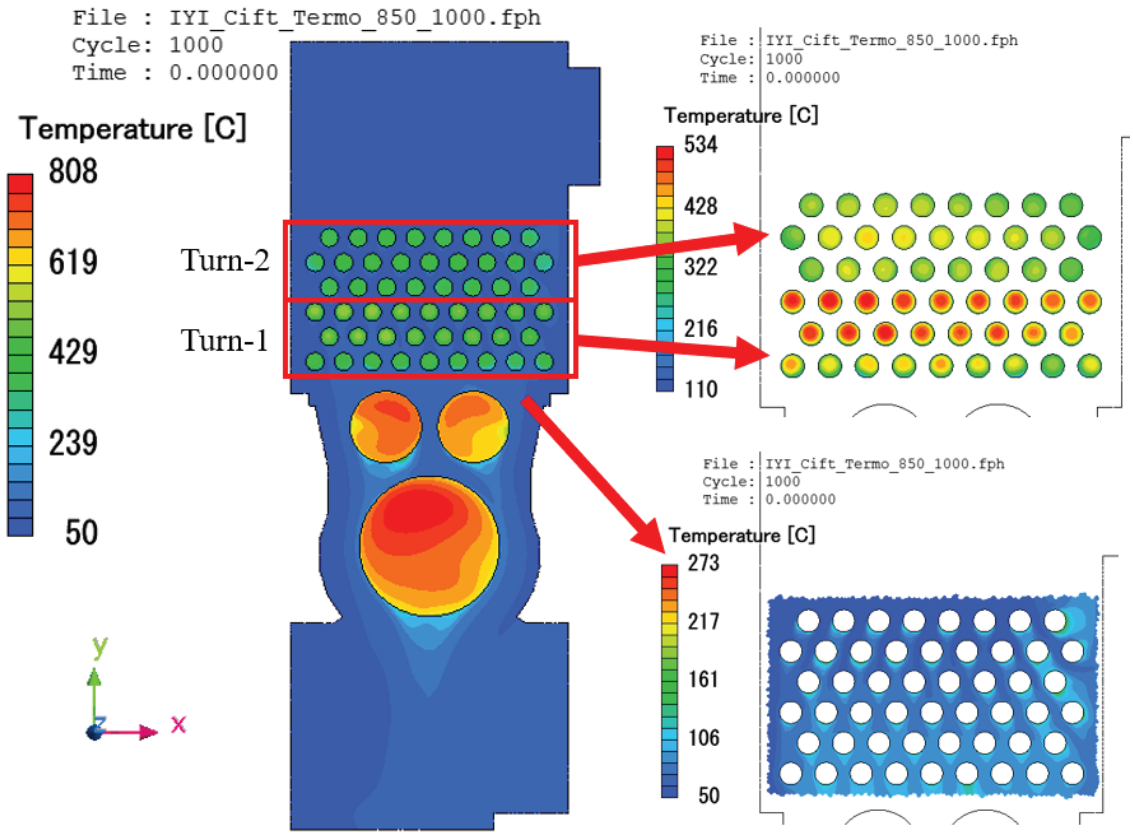

Figure 2.29. Temperature counters of the flow volumes perpendicular to mid-plane.

Both the surface temperatures and the mass flow rates in the pipes are not homogeneously distributed (Figure 2.30. and Figure 2.31.). This study argues that non-homogeneously distributed surface temperatures increase thermal stress due to different expand forces. Figure 2.30. shows that the mass flow rates in the pipes in the first line of the turn sections are lower than in the other lines. At the same time, the mass flow rates of the pipes in the last line in the same turn sections are higher than the other lines. At the points where the flow turns abruptly, the flow was not directed to the nearest pipes; instead, it was more easily directed to the pipes farthest from the turn.

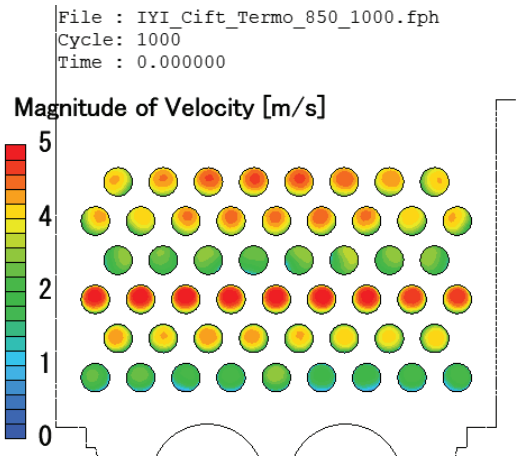

Figure 2.30. Flow velocities of the fluid in the heat exchanger

Figure 2.31. shows that the temperatures on the pipe surfaces are distributed non-homogeneously, and sudden temperature changes are observed both between the pipes and on their surfaces.

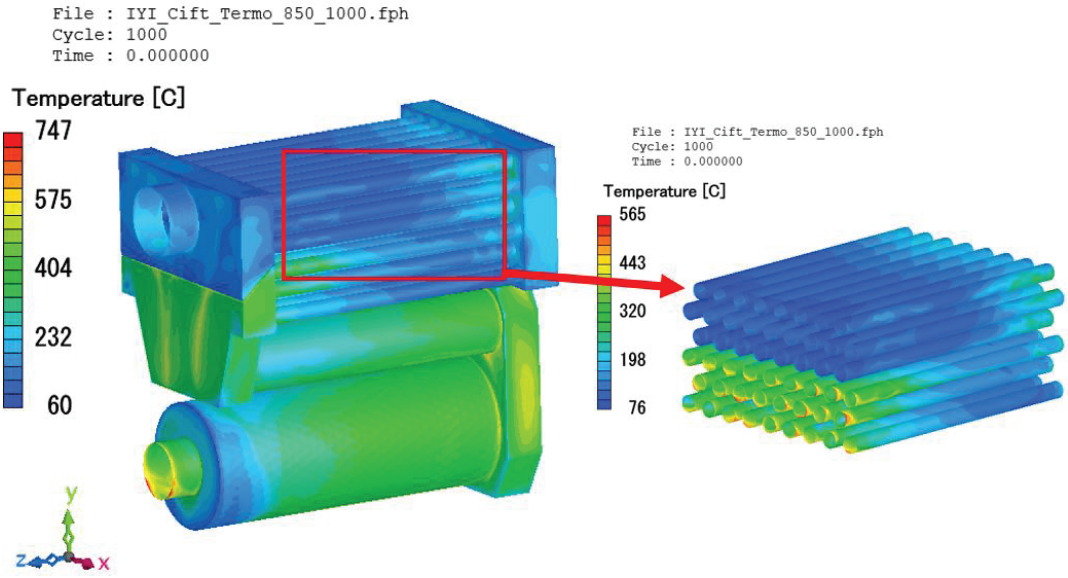

Figure 2.31. Surface temperatures of the heat transfer pipes

There are 26 heat transfer pipes in the first turn of the heat exchanger and 25 pipes in the second turn (Figure 2.29.). In Figure 2.32., the area-weighted mass flow rates (kg/s) on the outlet surfaces of the pipes located in the turn sections are shown. The relevant values are colored according to the values in that turn section to show the difference between the mass flow rates. Due to evaluating the mass flow rate in each pipe according to the average flow value of its turn, green color means more than average, yellow color means average value, and red color means less than average value.

	9	8	7	6	5	4	3	2	1	
TURN-2		0.010238	0.01102	0.011503	0.011771	0.011833	0.01154	0.011037	0.01022	3
	0.009872	0.010065	0.010989	0.011219	0.01102	0.011282	0.010995	0.010071	0.009979	2
		0.007889	0.007686	0.007965	0.007365	0.007426	0.007997	0.007653	0.007836	1
TURN-1	0.01196	0.012177	0.012331	0.012367	0.01252	0.012504	0.012437	0.012167	0.011987	3
		0.009688	0.009752	0.009824	0.010386	0.010333	0.009706	0.009753	0.009691	2
	0.006502	0.006294	0.005938	0.005706	0.008196	0.005593	0.005927	0.006332	0.006527	1
	1	2	3	4	5	6	7	8	9	

Figure 2.32. Mass flow rates of air in the heat transfer pipes section [Kg/s]

A mass flow rate of 0.253 kg/s passes through each turn section due to the conservation of mass. When the mass flow rates in the pipes are obtained as homogeneously distributed, the ideal mass flow rate ($\dot{m}_{Ideal}$, Kg/s) passing through them; directly depends on the total mass flow rate of the fluid entering the turn section and the total number of pipes (N_{Pipes}) in the turn section (15).

$$\dot{m}_{Ideal} = \frac{0.253}{N_{Pipes}} \tag{15}$$

Figure 2.33. shows deviations of the pipe's mass flow rates in each turn section from the ideal mass flow rate. The colors show positive or negative deviations. Flow rates that differ from the ideal rate in the positive direction are marked in green, rates close to the ideal rate are in yellow, and those that deviate in the negative direction are marked in red. The first turn section has 26 pipes, and the second turn section has 25 pipes.

	9	8	7	6	5	4	3	2	1	
TURN-2		1%	8%	12%	14%	14%	12%	8%	1%	3
	-3%	-1%	8%	10%	8%	10%	8%	0%	-1%	2
		-28%	-32%	-27%	-37%	-36%	-27%	-32%	-29%	1
TURN-1	19%	20%	21%	21%	22%	22%	22%	20%	19%	3
		0%	0%	1%	6%	6%	0%	0%	0%	2
	-50%	-55%	-64%	-71%	-19%	-74%	-64%	-54%	-49%	1
	1	2	3	4	5	6	7	8	9	

Figure 2.33. Deviation of the mass flow rates from ideal mass flow rates

The Mass Flow Rate Ratio ($\dot{m}_{Ratio}$, unitless) was calculated to document the non-homogeneous distribution more clearly in mass flow rates in the pipes. This ratio is calculated by dividing the pipe's mass flow rate by that turn section's ideal mass flow rate. The desired value of this ratio is 1 (red line). This ratio is calculated (16) for each pipe and plotted in Figure 2.34..

$$\dot{m}_{Ratio} = \frac{\dot{m}_{Pipe}}{\dot{m}_{Ideal}} \tag{16}$$

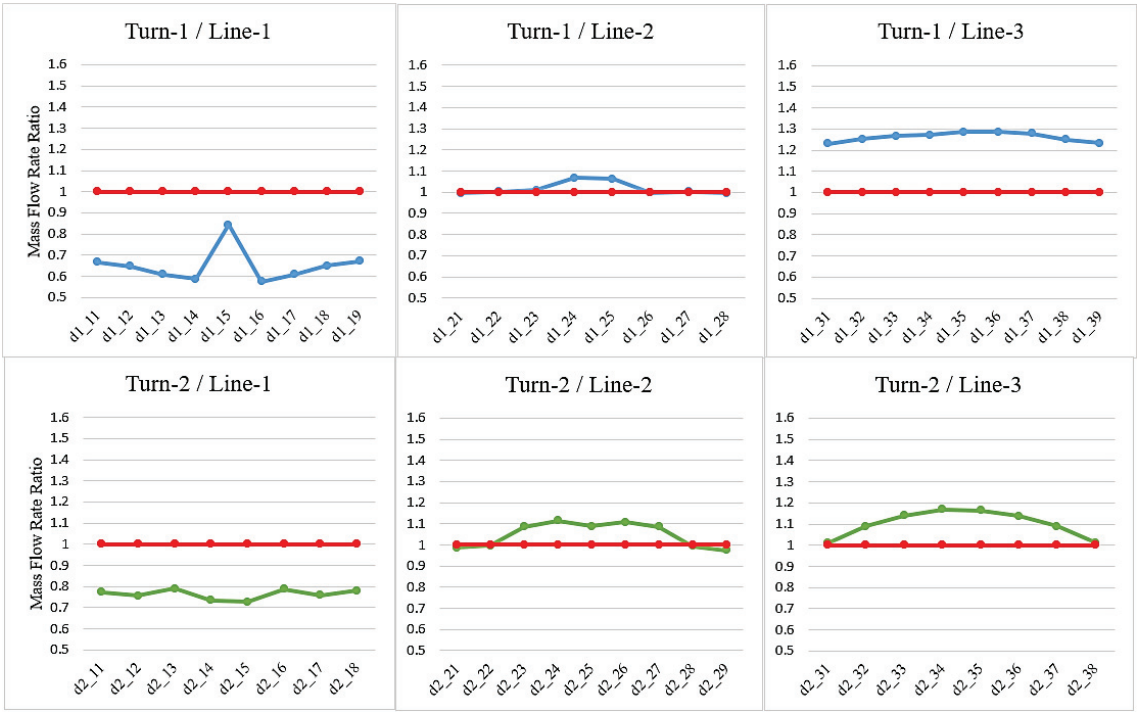

Figure 2.34. Mass flow rate ratio values in the heat transfer pipes

Average surface temperatures on the pipe surfaces are shown in Figure 2.35.. The non-homogeneous surface temperatures depend on the flow irregularity in the heat exchanger and the way the external flow passes over the heat exchanger. While the average surface temperature of the heat transfer pipes with a high mass flow rate is high, the surface temperatures of the heat transfer pipes with a low mass flow rate are low. As mentioned before, non-homogeneous surface temperatures increase thermal stresses.

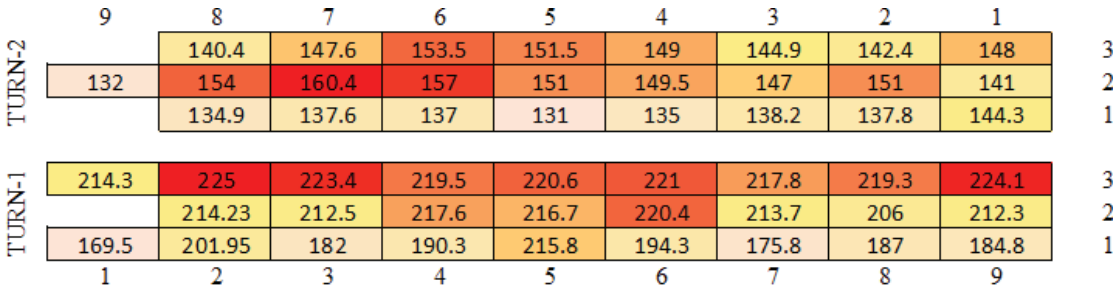

Figure 2.35. Average surface temperatures of the heat transfer pipes (°C)

A structural analysis model including the 2D surface model of the current heat exchanger design has been established to observe the thermal stresses. Since the general purpose of the study is to present the difference in the improvement to be made, the heat transfer pipe material P236GH (Table 2.9.) properties have been assigned to the overall model, and it has been assumed that this material entirely makes the heat exchanger. Surface temperatures obtained from the CFD solution are mapped onto the 2-D structural heat exchanger model (mesh), which covers the "wall_hex" (Figure 2.22.) surface definition exactly. As shown in Figure 2.36., the heat exchanger is fixed from the sides and edges of the chimney to simulate its actual placement inside the thermoblock. The thermal stress analysis of the structural model was solved in MSC Nastran software, and the maximum stresses were read.

Table 2.9. Mechanical properties of P235GH material [15]

Material	Elastic Modulus [GPa]	Shear Strength [MPa]	Thermal Expansion [µm/m.K]
P235GH	190	270	12

In the FEA analysis results, the maximum stress is 13 GPa (Figure 2.37.). The maximum stress shows that the structure has undergone plastic deformation (failure). A more precise structural analysis can be achieved with more accurate material identification and precise meshing. However, since this study aims to document the difference between the two models, the improved geometry will also be analyzed for exactly the same conditions.

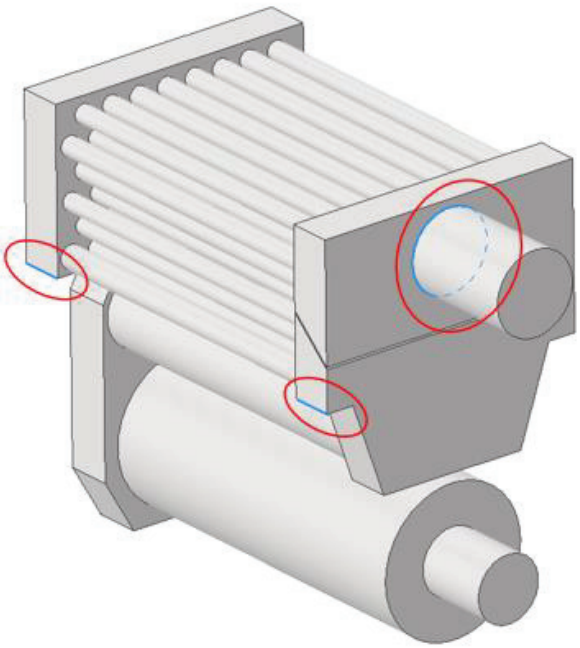

Figure 2.36. Fixed edges (symmetrical) of the heat exchanger for FEA simulation

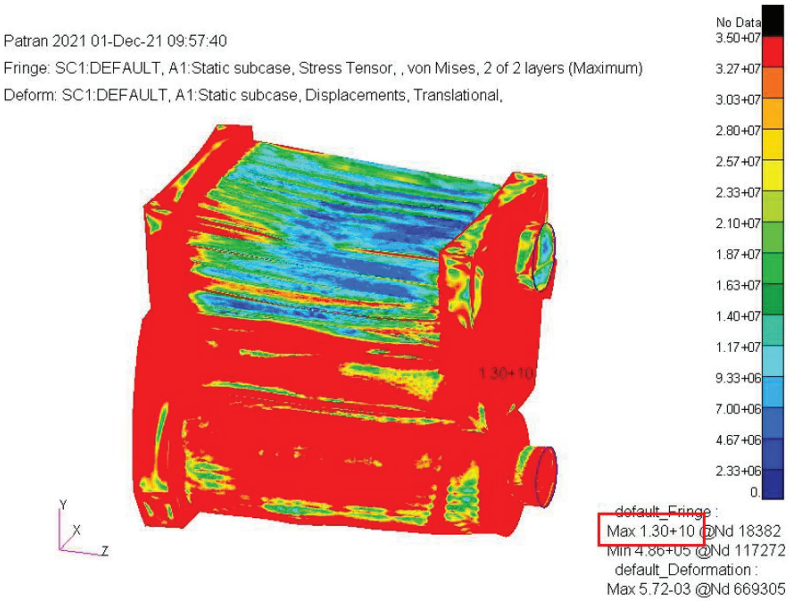

Figure 2.37. FEA thermal stress analysis of the current-state model with maximum stress [Pa]

A homogeneous temperature distribution will be provided on the pipe surfaces to reduce the thermal stresses. The main goal for this desired situation is to converge the mass flow rate values that deviate from the ideal mass flow value by −74% and +22% to the ideal mass flow rate value.

CHAPTER 3

RESULTS

This study aims to reduce the thermal stresses by distributing the surface temperatures of the heat transfer pipes homogeneously. The current-state analysis has shown that one of the most critical factors of this phenomenon is the deviation of the flow rates in the pipes from the ideal flow rate.

Poiseuille's Law (17) was considered to improve the flow rates [26]. This equation, used to calculate the volumetric flow rate, shows us that a change in the flow diameter affects the volumetric flow rate (assumed that other parameters are constant) by four times over the change. Increasing and decreasing the pipe diameters have changed the pipe flow resistances and made the fluid flow rates closer to the ideal value.

$$\dot{V} = \frac{\Delta P \times \pi \times D^4}{128 \times \mu \times L} \; [m^3/s] \tag{17}$$

Improvement study on pipe diameters was performed only in the heat exchanger flow volume (without external flow, Figure 3.1.). After obtaining the improved values, the improved-state will also be analyzed by using the boundary conditions of the current-state analysis.

The energy equations were not solved in the analyzes in which only the diameter changes were made to obtain results for the study in a shorter time.

To focus on the study's goal; it is aimed at the improved geometry that the maximum deviation between the mass flow rates of the pipes and the ideal mass flow rate values is 10%.

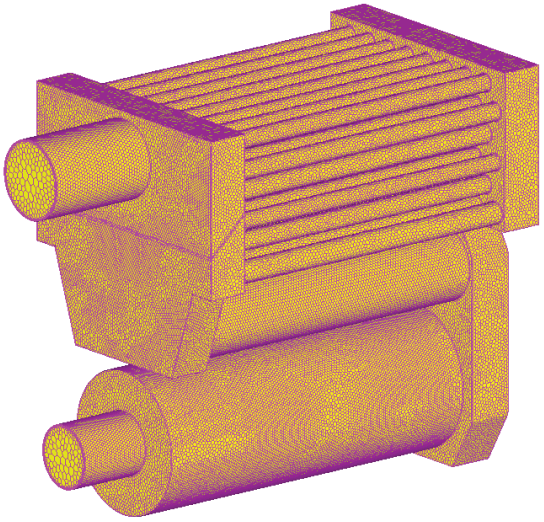

Figure 3.1. Control volume of the optimization study (with mesh)

In order to reduce the non-computational factors in the results, mesh dependency of the model was tested for pressure difference in the heat exchanger. As a result of this study, the least element number was decided, which documents similar results by a more refined mesh structure (Figure 3.2.).

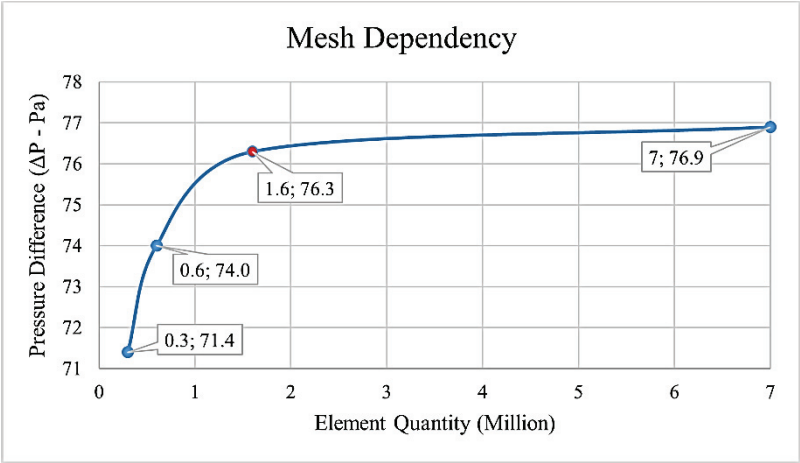

Figure 3.2. Results of the mesh dependency test

As a result of the mesh dependency test, it was decided to continue the study with a 1.6 million polyhedral mesh element. Regarding optimization studies, the diameters of the pipes that have more flow rate than the theoretical flow rate average were reduced, and the diameters of those with less flow rate were increased (Figure 3.3.). Thus, the flow resistances in the heat transfer pipes are arranged. The flow resistance decreases in pipes with increased diameter, while the resistance increases in pipes with reduced diameter. Changing pipe diameter also affected the amount of flow directed to that pipe.

As shown in Figure 3.3., increasing and decreasing the pipe diameters was carried out. First, focused on the pipes that deviate the most from the ideal mass flow rate. The diameter changes were performed through an iterative study. After each diameter change, the flow analyzes without energy equations were run. After interpretation of the results, new changes were made to the previous diameter changes and studied again. The figure documents increased diameter ratios in green and decreased diameter ratios in red.

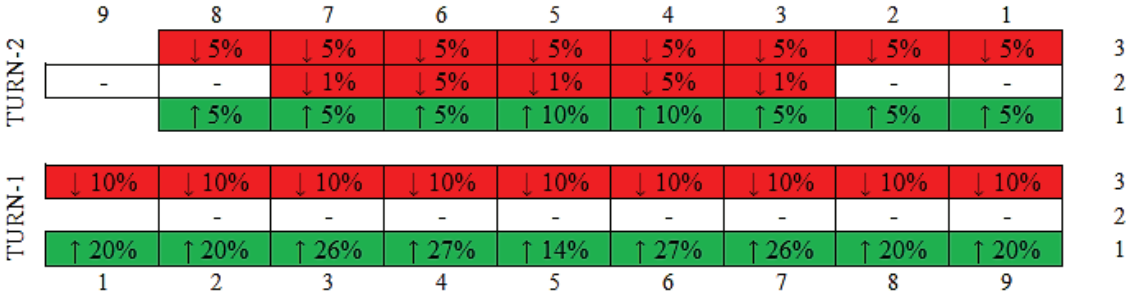

Figure 3.3. Diameter change ratio of the pipes

After the final diameter changes were decided, the analysis model with the exact conditions of the current-state analysis and the external flow volume was recalculated. As the convergence criteria, 10^{-5} relative fluctuation is determined. The convergence value decreased below 10^{-5} relative fluctuation during the analysis, and it was stopped at that 1445^{th} cycle (Figure 3.4.).

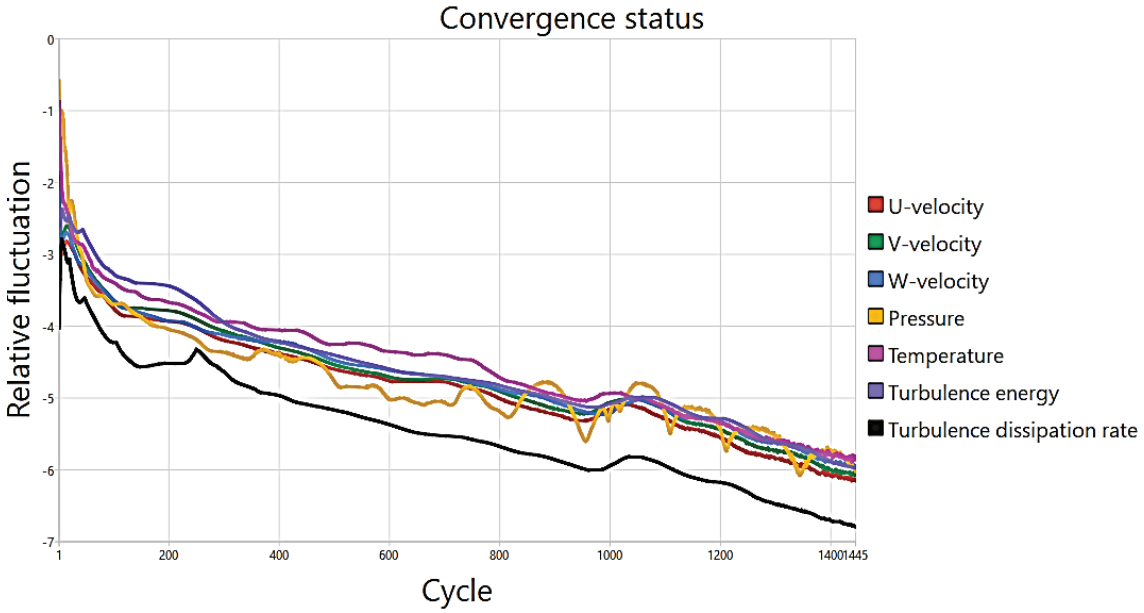

Figure 3.4. Convergence graph of the improved-state analysis

Inlet-outlet temperatures and pressure difference values were recalculated to see how the geometry changes affected the outputs of the analysis. As seen in Table 3.1., there was no change in the inlet and outlet temperatures. As a result of the changes made in the pipe diameters, the flow resistances were both decreased and increased. Therefore, the pressure difference in the heat exchanger is reduced by only 2.2 Pa.

Table 3.1. Outputs of the improved model

Condition	Output
HEX Inlet Temperature	850 °C
HEX Outlet Temperature	280.5 °C
Thermoblock Inlet Temperature	50 °C
Thermoblock Outlet Temperature	98 °C
Pressure Difference in HEX (ΔP)	55.5 Pa

As shown in Figure 3.5., the temperature differences between the lines decreased at the inside pipe temperatures (especially for the same turn section). Fluid temperatures of the pipes in the turn sections are distributed more homogeneously, and transition of the surface temperatures between pipes more smoothly.

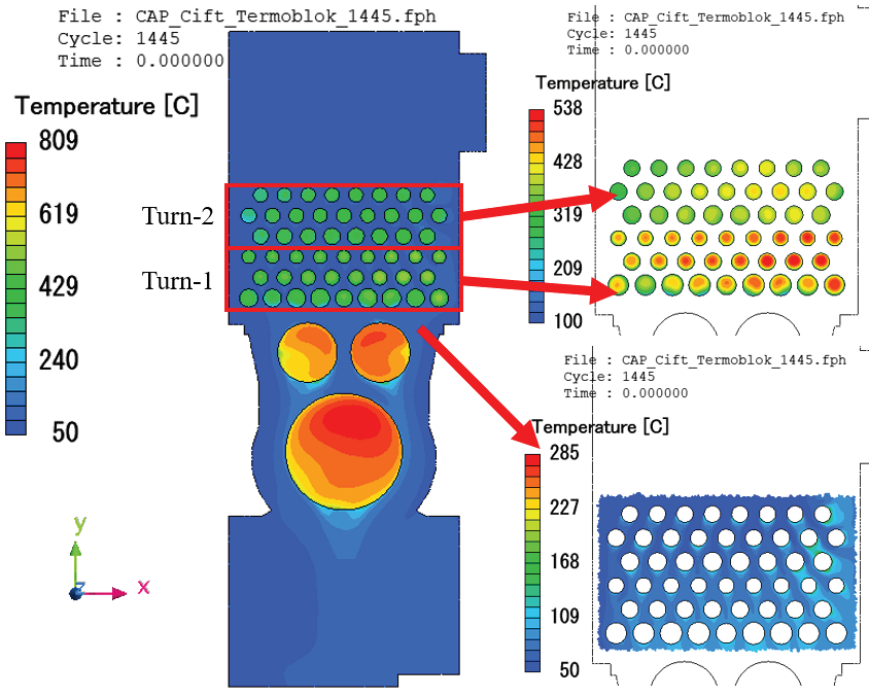

Figure 3.5. Fluid temperatures in the thermoblock and heat exchanger volumes with improved geometry (improved-state)

When the flow rates in the heat exchanger are examined carefully, it is observed that a smoother surface temperature transition is provided between the lines in the same turn sections compared to the current-state (Figure 3.6.). Although the flow velocity distributions in the pipes seem different, the most significant difference from the current-state is that the pipe diameters are different. For this reason, reading high flow velocities in small pipe diameters and low flow velocities in large pipe diameters shows that the mass flow rate distribution is homogenized.

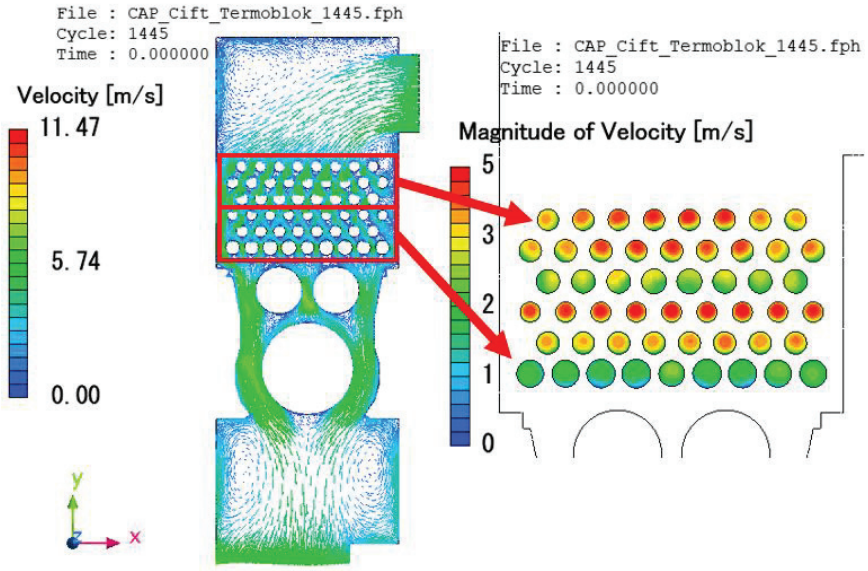

Figure 3.6 Velocity vectors of the outer flow and flow velocities in the heat exchanger (improved-state)

As shown in Figure 3.7., the mass flow rate distribution in the heat transfer pipes is homogenized. The sharp mass flow rate differences observed in the current-state are smoothed out.

	9	8	7	6	5	4	3	2	1	
TURN-2		0.009164	0.00987	0.010131	0.010379	0.010366	0.010359	0.009977	0.009363	3
	0.010248	0.010249	0.010889	0.010367	0.01096	0.010402	0.010938	0.010288	0.010242	2
		0.009423	0.009441	0.009936	0.010683	0.010672	0.009653	0.009459	0.009541	1
TURN-1	0.009368	0.009501	0.009356	0.009888	0.00998	0.009793	0.009432	0.009677	0.009391	3
		0.009995	0.009796	0.010231	0.010403	0.010275	0.010197	0.009962	0.010009	2
	0.010085	0.010008	0.009219	0.00911	0.010039	0.008855	0.009227	0.009551	0.009652	1
	1	2	3	4	5	6	7	8	9	

Figure 3.7. Mass flow rates of air in the heat transfer pipes section (improved-state) [kg/s]

As a result of the study, the maximum deviation of the mass flow rates in the heat transfer pipes between the ideal mass flow rate value is ±10% (Figure 3.8.).

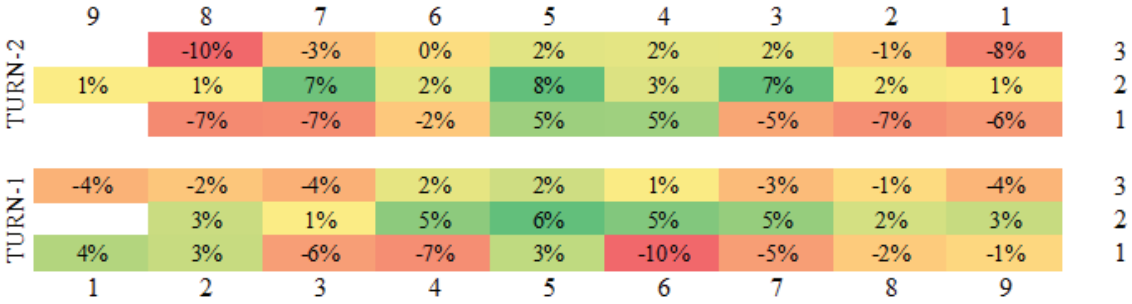

Figure 3.8. Deviation of the flow rates from ideal rates (improved-state)

With the improvement studies on the heat transfer pipe diameters, the mass flow rate distributions in the pipes have converged to the ideal value. As mentioned before, the ideal value of the mass flow rate ratio in the pipe is 1. While the current mass flow rate ratios (Figure 2.34.) are far from 1, ratios that are very close to 1 have been obtained with the improvement (Figure 3.9).

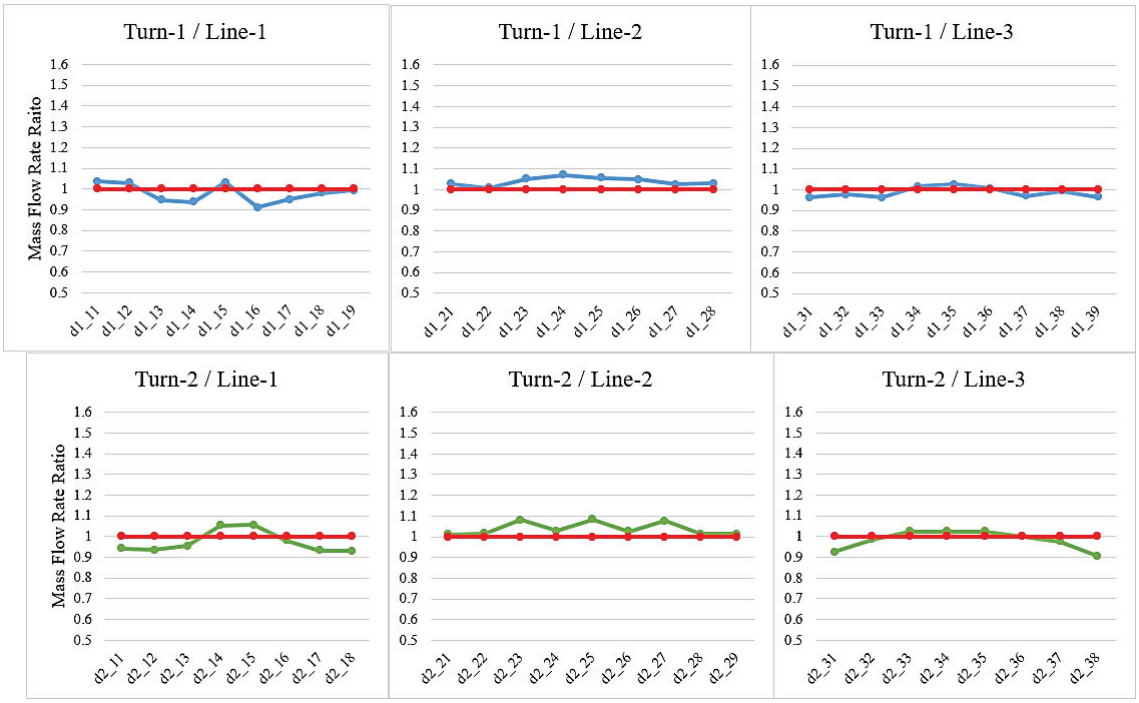

Figure 3.9. Mass flow rate ratio values in the heat transfer pipes (improved-state)

With the achievement of this goal, smoother temperature transitions and lower temperature differences are observed in the pipe surface temperatures (Figure 3.10.)

compared to the previous design (Figure 2.35.). The temperature distribution in the turn sections decreases from left to right because of the undirected flow in the thermoblock.

	9	8	7	6	5	4	3	2	1	
TURN-2		125.3	134	143.5	146.4	153.8	157	147.7	154.4	3
	120.1	142.6	151.6	153	150.8	150	154	162	155.4	2
		131.8	135	138.5	138	136.8	144.5	149.8	157.8	1
TURN-1	188.6	200	203	211.5	213	214	222	228.8	229.3	3
		194.6	196.5	209	213.6	217	223	227	233.5	2
	159.6	179	181.5	187	213	198	191	215.5	193.7	1
	1	2	3	4	5	6	7	8	9	

Figure 3.10. Average surface temperatures of the heat transfer pipes (improved-state) [°C]

At the beginning of this study, it was observed that the temperature differences on the heat exchanger surface caused various thermal stresses by using the results of the CFD simulations in the FEA analysis. To confirm that these stresses will decrease due to homogenous surface temperature distribution, the FEA analysis, which includes the same conditions, was performed by mapping the surface temperatures obtained from CFD analysis on the improved geometry model.

As a result of the improvement/optimization study, the maximum stress value of 13 GP decreased to 9.88 GPa (Figure 3.11.). Reducing the temperature differences on the heat exchanger surface also reduced the thermal stresses by 24%.

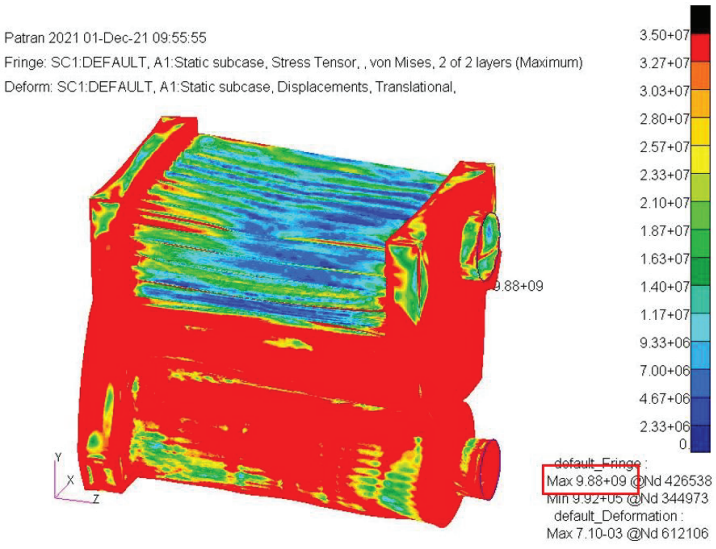

Figure 3.11. FEA thermal stress analysis of improved model

CHAPTER 4

CONCLUSION

This thesis documents that thermal stresses in the considered heat exchanger can be reduced by homogenizing the surface temperature distribution. First, the heat exchanger and its inner (internal) and outer (external) flow volumes were modeled. A gas-fired burner is used for the heat source in the current state. Since the thermophysical properties of the flue gases are very close to the air, both inner and outer fluids were defined as air. The results obtained from the current-state study are in agreement with the test results. The current-state analyses have shown a non-homogeneous distribution in the surface temperatures and critical deviation from the ideal flow rate in the flow rates in the heat exchanger. These deviations vary between −74% and +22%. In addition, the surface temperature values obtained from the current-state analyzes were mapped to the structural analysis model of the current-state geometry. In the structural analysis, the material of the heat transfer pipes, P235GH, was defined as the material for the whole geometry. The assumptions are based on the fact that this is a comparison study, and the main aim is to present the difference between the two states. In the thermal analysis carried out considering the mounting conditions in the volume where the heat exchanger is located, it has been observed that the design has undergone plastic deformation due to thermal stresses. In order to decrease thermal stresses, it was first tried to obtain the ideal mass flow rate in the pipes of the heat exchanger. A maximum ±10% deviation of the pipe mass flow rate from the ideal mass flow rate is targeted for the success of this study. It was decided to arrange the flow resistances to obtain homogeneously distributed mass flow rates and surface temperatures in the heat exchanger pipes. The resistances are set by increasing or decreasing the pipe diameters as a percentage according to the initial size. Thus, the pipe diameter with more mass flow rate than the ideal mass flow rate is reduced while the pipe diameter with less mass flow rate is increased. Changing the pipe diameters is provided a maximum ±10% deviation of the mass flow rate from the ideal mass flow rate in the heat transfer pipe sections. The improved geometry was simulated again with the exact conditions of the current-state.

The results show that the surface temperatures are distributed more homogeneously due to the geometry improvement, and the temperature transitions are smoother than in the current-state. The maximum thermal stress value in the heat exchanger was reduced by 24%. In addition, the study was not provided an improvement in the thermal efficiency (outlet temperatures) or the amount of pressure loss of the heat exchanger. Changing pipe placement, adding a fin geometry before the turn sections, or a different model design based on external flow can be suggested to reduce thermal stresses further.

REFERENCES

[1] Gutowski, S., 2013, “From Nature’s Designs to Advanced Sustainable Coatings,” p. 7.

[2] Du, Z., Wen, S., Wang, J., Yin, C., Yu, D., and Luo, J., 2016, “The Review of Powder Coatings,” J. Mater. Sci. Chem. Eng., **04**(03), pp. 54–59.

[3] Paint & Coatings Industry Magazine, 2004, “Enlarging the Cure Window of Powder Coatings.”

[4] Mitsuba Systems (India) PVT LTD, “Pretreatment for Powder Coating.”

[5] Adullah, S., and Ezuber, H. M., 2011, “Repair of Tube–Tubesheet Weld Cracks in a Cracked Gas/Steam Heat Exchanger,” J. Fail. Anal. Prev., **11**(6), pp. 611–617.

[6] Matsumori, T., Kawamoto, A., and Kondoh, T., 2019, “Topology Optimization for Thermal Stress Reduction in Power Semiconductor Module,” Struct. Multidiscip. Optim., **60**(6), pp. 2615–2620.

[7] Gocmen, S., Gungor, S., and Cetkin, E., 2020, “Thermal Management of Electric Vehicle Battery Cells with Homogeneous Coolant and Temperature Distribution,” J. Appl. Phys., **127**(23), p. 234902.

[8] Cetkin, E., 2017, “Constructal Microdevice Manifold Design With Uniform Flow Rate Distribution by Consideration of the Tree-Branching Rule of Leonardo Da Vinci and Hess–Murray Rule,” J. Heat Transf., **139**(8), p. 082401.

[9] 2020, “Flue Gases Properties Table, ‘Www.Pipeflowcalculations.Com/Tables/Flue-Gas.Xhtml.’”

[10] 2020, “Air Properties Table at 1 Bar, ‘Www.Pipeflowcalculations.Com/Tables/Air.Xhtml.’”

[11] Bergman, T., Lavine, A., Incropera, F., and Dewitt, D., 2013, “One-Dimensional Steady-State Conduction,” *Fundamentals Heat and Mass Transfer, 7th Edition*, U.S.A, p. 116.

[12] “Properties of 202 Stainless Steel, Annealed Plate, Sheet, Strip, Http://Www.Matweb.Com/.”

[13] “Rock Wool, Thermal Conductivity, Www.Engineeringtoolbox.Com.”

[14] Kosky, P., Balmer, R., Keat, W., and Wise, G., 2013, “Mechanical Engineering, Table 12.2,” *Exploring Engineering*, Elsevier, pp. 259–281.

[15] “Properties of EN 1.0345 (P235GH) Non-Alloy Steel, Www.Makeitfrom.Com.”

[16] Kakac, S., and Liu, H., 2002, “Overall Heat Transfer Cofficient,” *Heat Exchangers - Selection, Rating and Thermal Design*, CRC PRESS, U.S.A., p. 39.

[17] Kakac, S., and Liu, H., 2002, “Hydraulic Diameter,” *Heat Exchangers - Selection, Rating and Thermal Design*, CRC PRESS, U.S.A., p. 87.

[18] Kakac, S., and Liu, H., 2002, “Reynolds Number,” *Heat Exchangers - Selection, Rating and Thermal Design*, CRC PRESS, U.S.A., p. 91.

[19] “Air Dynamic and Kinematic Viscosity - Www.Engineeringtoolbox.Com.”

[20] “Air Density vs. Temperature, Www.Engineeringtoolbox.Com.”

[21] Mroue, H., 2018, “Numerical and Experimental Investigation of a Multi-Pass Heatpipe-Based Heat Exchanger,” Doctor of Philosophy Thesis, Brunel University London.

[22] Kan, M. D., “Yanma Gaz Analizleri ve Dogalgaz Uygulamalarindaki Onemi,” p. 17.

[23] Önder, D., “Dogal Gaz Genel Bilgiler,” p. 7.

[24] Cengel, Y., and Boles, M., 2015, *Thermodynamics: An Engineering Approach, Eighth Edition, Appendix Table A-17*, McGraw-Hill Education, U.S.A.

[25] 2013, “Polyhedral, Tetrahedral and Hexahedral Mesh Comparison, ‘Www.Symscape.Com/Polyhedral-Tetrahedral-Hexahedral-Mesh-Comparison.’”

[26] Cengel, Y., and Cimbala, J., 2006, “Poiseuille’s Law,” *Fluid Mechanics*, McGraw-Hill Education, U.S.A., p. 330.